nature neuroscience

Article

https://doi.org/10.1038/s41593-025-01966-7

Lemborexant ameliorates tau-mediated sleep loss and neurodegeneration in males in a mouse model of tauopathy

Received: 23 November 2022

Accepted: 2 April 2025

Published online: 27 May 2025

Check for updates

Samira Parhizkar ¹, Xin Bao¹, Wei Chen¹, Nicholas Rensing¹, Yun Chen¹, Michal Kipnis¹, Sihui Song¹, Grace Gent¹, Eric Tycksen ², Melissa Manis ¹, Choonghee Lee¹, Javier Remolina Serrano¹, Megan E. Bosch¹, Emily Franke¹, Carla M. Yuede ^{13,4}, Eric C. Landsness¹, Michael Wong¹ & David M. Holtzman ¹

Sleep disturbances are associated with the pathogenesis of neurodegenerative diseases such as Alzheimer's disease and primary tauopathies. Here we demonstrate that administration of the dual orexin receptor antagonist lemborexant in the P301S/E4 mouse model of tauopathy improves tau-associated impairments in sleep—wake behavior. It also protects against chronic reactive microgliosis and brain atrophy in male P301S/E4 mice by preventing abnormal phosphorylation of tau. These neuroprotective effects in males were not observed after administration of the nonorexinergic drug zolpidem that similarly promoted nonrapid eye movement sleep. Furthermore, both genetic ablation of orexin receptor 2 and lemborexant treatment reduced wakefulness and decreased seeding and spreading of phosphorylated tau in the brain of wild-type mice. These findings raise the therapeutic potential of targeting sleep by orexin receptor antagonism to prevent abnormal tau phosphorylation and limit tau-induced damage.

Sleep loss, including a substantial decrease in nonrapid eye movement (NREM) sleep and rapid eye movement (REM) sleep time, is associated with increased risk of Alzheimer's disease (AD), the most common neurodegenerative disease, by up to fourfold^{1,2}. While several classes of hypnotics are commonly prescribed for managing sleep impairments, there are currently no sleep—wake-targeting medications aimed at modifying disease pathology in neurodegenerative diseases. In addition to potentially being causative, sleep—wake disturbances are observed in individuals with symptomatic AD and other tauopathies, such as progressive supranuclear palsy (PSP) and corticobasal degeneration (CBD), most likely due to accumulation of abnormally phosphorylated tau (pTau)—an intracellular microtubule-associated protein—in

brain regions that control key sleep—wake pathways³-6. This abnormal hyperphosphorylation at specific sites of tau reduces microtubule binding, substantially increasing the propensity of self-assembly and formation of paired helical filaments (PHFs) as well as neurofibrillary tangles associated with neuronal loss and cognitive decline⁷. Decreased NREM sleep is associated with tau pathology at the earliest stages of cognitive decline, with sleep quality decreasing with the severity of tau pathology³.9. Our lab has reported that sleep loss in humans and mice, or chemogenetically induced increased wakefulness in mice, increases interstitial and cerebrospinal fluid tau levels due to increased production or release of tau through excitatory neuronal activitys³.10. In addition, we and others have also shown that sleep disruption acutely

¹Department of Neurology, Hope Center for Neurological Disorders, Knight Alzheimer's Disease Research Center, Washington University School of Medicine, St. Louis, MO, USA. ²Genome Technology Access Center, Washington University School of Medicine, St. Louis, MO, USA. ³Department of Psychiatry, Washington University School of Medicine, St. Louis, MO, USA. ⁴Department of Neuroscience, Washington University School of Medicine, St. Louis, MO, USA. Mo, US

increases the accumulation and spreading of tau pathology^{10,11}. These studies suggest that changes in tau deposition introduced by sleep—wake disturbances may directly influence a disease-damaging trajectory leading to neurodegeneration. Whether treatments targeting sleep could potentially offer neuroprotection has yet to be determined.

The efficacy limitations and side effects of existing insomnia medications have driven the need to develop new therapeutic approaches for managing sleep disorders. For instance, while sleep-wake modulating drugs such as the gamma-aminobutyric acid-A (GABA_A) receptor-positive allosteric modulator zolpidem, benzodiazepine triazolam or antihistaminergic doxylamine are effective in managing symptoms related to sleep onset and dysfunction, most of these are unsuitable for patients with neurodegenerative disorders. This is especially the case for the elderly who are at risk of dementia because of the reported side effects associated with motor incoordination as well as memory impairment¹²⁻¹⁵. Besides these hypnotics, dual orexin receptor antagonists (DORA) that target hypervigilance are also used to treat insomnia in adults. Orexins are neuropeptides that bind and activate their associated G-protein-coupled receptors (GPCR), orexin receptor 1 (OXR1; Hcrtr1) and OXR2 (Hcrtr2). Selective orexin receptor (OXR) antagonism of OXR1 results in changes in feeding, reward, emotion and motivation, whereas selective inhibition of OXR2 directly impacts sleep-wake regulation^{16,17}. While orexin-expressing neurons are confined to the lateral hypothalamus in the brain, these neurons project to numerous sleep- and wake-controlling nuclei as well as to the hippocampus and neocortex, regions that contain pTau pathology in both early and late stages of AD³. In fact, in humans, pathological pTau is observed as early as Braak stage 0 in wake-promoting neurons, including orexinergic neurons in the arousal network across tauopathies^{4,5}. Therefore, therapeutically targeting these pathological changes early in the disease, when sleep disturbances first emerge, could potentially help prevent further damage and the progression to advanced neurodegeneration. Currently, suvorexant and lemborexant are the only DORAs clinically investigated in patients with AD and insomnia disorder or irregular sleep-wake rhythm disorder, respectively, which have been shown to ameliorate sleep loss without exacerbating or improving underlying cognitive impairment^{18,19}. Additionally, suvorexant has been shown to reduce amyloid-β (Aβ) and pTau181 in CSF over hours compared to placebo-treated cases²⁰. Lemborexant, which preferentially binds to OXR2, has been shown to effectively promote sleep in both mice and humans 19,21-23, without potentiating sedative effects, appetite-induced weight gain or impairing motor coordination associated with hypnotics¹⁵. These findings strongly support the need to explore DORAs as a potential therapeutic option for treating both sleep disturbances and pathophysiological changes associated with neurodegenerative diseases.

Our group has previously demonstrated that increasing sleep through genetic removal or pharmacological antagonism of OXRs directly influences $A\beta$ pathology 24,25 . However, $A\beta$ deposition in and of itself is not directly linked with the rate of brain atrophy or neuronal loss 26 . The P301S/E4 mouse model of tauopathy 27 exhibits accelerated tau accumulation beginning at 5-6 months of age, with substantial neuroinflammation and regional brain atrophy evident by 9.5 months. This acceleration in pathology is additionally driven by the expression of human APOE4—the strongest genetic risk factor for AD—in PS19 tau transgenic mice 28 . Using this mouse model, we aimed to assess whether sleep-promoting drugs, including zolpidem and lemborexant, could influence tau, associated sleep loss/hyperarousal, as well as chronic glial reactivity, regional brain atrophy and synapse loss that contribute to neurodegeneration and memory dysfunction 29,30 .

Results

Lemborexant and zolpidem increase NREM sleep

To compare the effects produced by both sleep-inducing treatment modalities on brain pathology, we orally gavaged P301S/E4 tauopathy

mice²⁷ daily with 30 mg kg⁻¹ zolpidem or lemborexant starting at 7.5 months for 2 months until 9.5 months. While zolpidem was gavaged at a single timepoint at zeitgeber time (ZT13), lemborexant was tested at ZT3 to increase sleep efficiency at a time when mice would normally be asleep during the light phase (ZT3), compared to reducing total wake time at the dark phase (ZT13). We found a tau-dependent reduction in NREM sleep and increased wake time in vehicle-treated P301S/E4 mice compared to E4 mice (Extended Data Fig. 1a), confirming that pathological tau is linked with disrupted sleep⁹. Lemborexant treatment increased NREM sleep by ~25% and reduced awake time by ~20% in both E4 and P301S/E4 mice (Extended Data Fig. 1a). Consistent with previous findings, both zolpidem (~30%) and lemborexant (~30% at ZT13 and ~15% at ZT3) increased sleep compared to vehicle when measured up to 4 h after time of administration (Fig. 1a). In line with previous reports^{21,31}, this increase was primarily driven by more time spent in NREM (Fig. 1b-d), with lembor exant at ZT13 significantly reducing wakefulness compared with vehicle (Fig. 1b) in P301S/E4 male mice. Similar changes in NREM sleep and wake percentage were also observed in female P301S/E4 mice (Extended Data Fig. 1b). The effects of lemborexant on sleep at both ZT3 (Fig. 1e) and ZT13 (Fig. 1f) lasted up to 5 h after administration and mostly returned to baseline by 7 h postgavage, without compensational phase delays. Lemborexant-treated mice displayed an improved consistency in sleep-wake behavior over 24 h compared with vehicle-treated P301S/E4 mice at corresponding timepoints, in addition to ameliorating tau-associated sleep-wake impairments. This was noted by a ~25% increase in NREM sleep and a ~20% reduction in wakefulness (Extended Data Fig. 1b). In summary, lemborexant as well as zolpidem effectively promoted sleep, with lemborexant providing longer-lasting effects on sleep-wake behavior over a 24-h period compared to zolpidem at a comparable dose.

Blocking orexin signaling is neuroprotective in males

We next investigated whether promoting sleep in the P301S/E4 mice could mitigate neurodegeneration (Fig. 2) that is associated with chronic neuroinflammation^{27,29}. In line with previous findings^{27,29,32}, vehicle-administered P301S/E4 mice displayed substantial brain atrophy compared to nontau transgenic E4 mice, evidenced by a marked reduction in hippocampal and entorhinal/piriform cortical volumes, as well as enlargement of the lateral ventricles (Fig. 2a,b). Given that female P301S/E4 display substantially less regional atrophy in the brain compared to their male counterparts, each sex was evaluated separately. Among the sleep-promoting agents, only mice treated with lemborexant showed protection against brain atrophy, with the most pronounced effects observed in the lemborexant-treated group at ZT13 (Fig. 2a-h). Notably, this neuroprotective effect was observed exclusively in male mice (Fig. 2c-h), with no significant effect detected in females (Fig. 2i-n). Ventricular volume was significantly reduced in lemborexant-treated male mice compared to those treated with zolpidem or vehicle (Fig. 2c). A similar pattern in the reduction of neuronal damage was further detailed by volumetric analysis of cresyl violet-stained tissue, showing a ~30-40% larger hippocampal volume and granule cell layer thickness in the dentate gyrus, as well as entorhinal/piriform cortex volume and pyramidal cell layer thickness (Fig. 2d-g) in lemborexant-treated group at ZT13 compared to controls. Similarly, although not significant, lemborexant-treated group at ZT13 showed a ~20% larger increase in each of these measures compared to controls. This striking attenuation of neurodegeneration was supported by reduced plasma neurofilament light chain levels (NfL) in males (Fig. 2h), validating a robust improvement in neuronal damage and degeneration. We hypothesized that the reduction in neuronal damage in the brain may improve memory-related impairments reported in P301S/E4 mice 27,32 . There were no significant differences in tone-shock (T/S) pairing or contextual and auditory cue conditioning behavioral paradigms (Extended Data Fig. 2a-c) in the lembor exant- or zolpidem-treated mice. However, we found a significant ~10% absolute

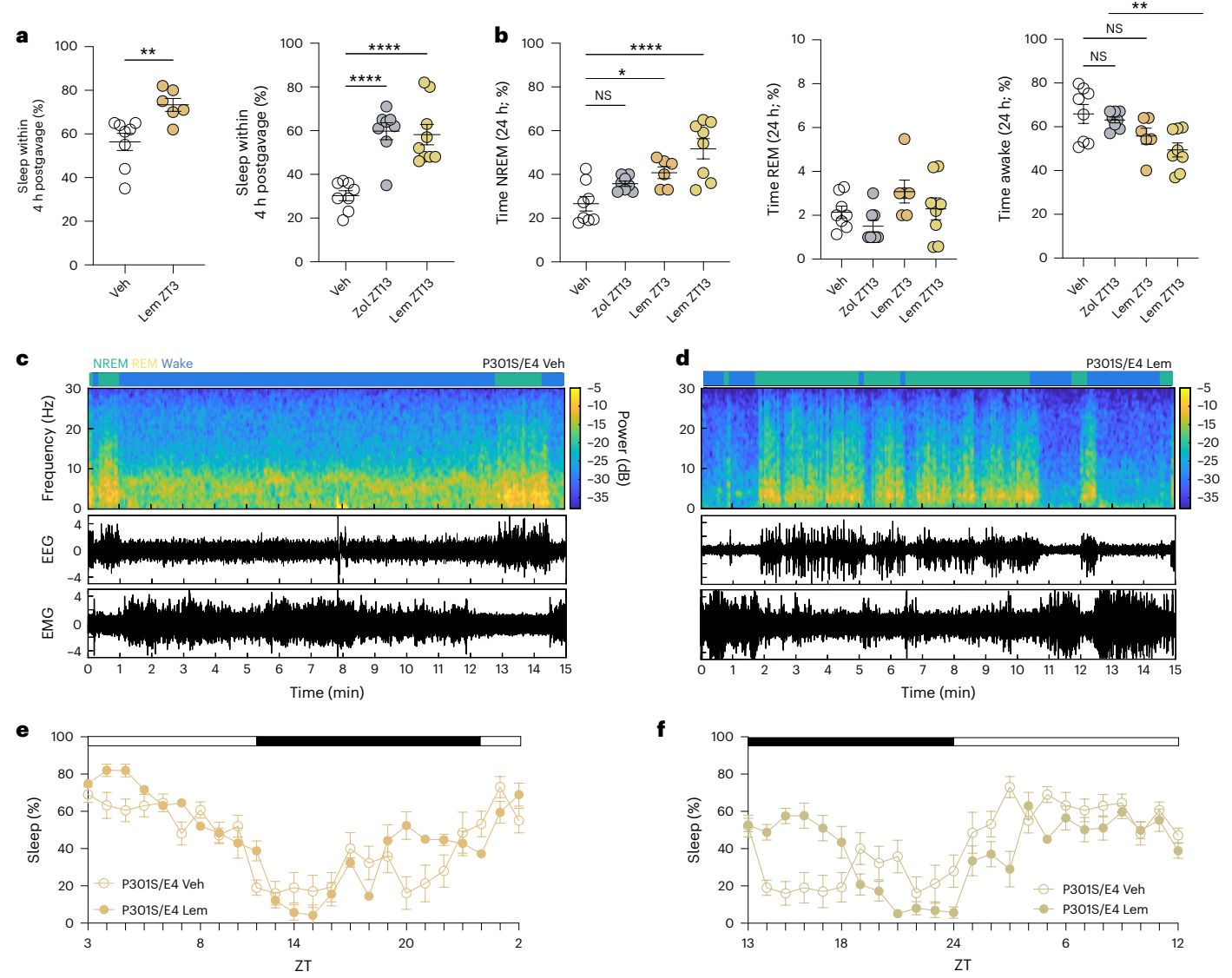


Fig. 1| **Zolpidem** and lemborexant treatment increase NREM sleep in male **P301S/E4 mice.** a, EEG analyses of percentage sleep in the first 4 h postgavage. Left: Lem gavage compared to vehicle gavage at ZT3 ($n_{\text{Veh}} = 8$, $n_{\text{Lem}ZT3} = 6$; two-tailed ttest). Right: Zol gavage and Lem gavage compared to vehicle gavage at ZT13 (n = 8 mice per group; one-way ANOVA, Dunnett's post hoc test). **b**, EEG analyses of percentage time spent in NREM sleep, REM sleep and awake during a 24 h period ($n_{\text{Veh}} = 8$, $n_{\text{Zol}ZT13} = 8$, $n_{\text{Lem}ZT3} = 6$, $n_{\text{Lem}ZT3} = 8$). One-way ANOVA, Dunnett's post hoc test. **c**, **d**, Representative EEG and EMG spectrograms

illustrating NREM, REM and wake patterns in Veh (c) and Lem-treated male mice (d). e, f, Percentage sleep observed over 24 h starting from time of gavage at ZT3 (e) and ZT13 (f; $n_{\text{Veh}} = 8$, $n_{\text{Lem}ZT3} = 6$, $n_{\text{Lem}ZT3} = 8$). White and black bars note the light phase and dark phase, respectively. For detailed statistical information, see Supplementary Table 1. Data represent mean \pm s.e.m. of biological replicates; *P < 0.05, **P < 0.01 and ****P < 0.0001. NS, not significant; Lem, lemborexant; Zol, zolpidem; Veh, vehicle.

increase in alternation rate in lembor exant-treated male groups, indicating an improvement in exploratory behavior compared to zolpidemor vehicle-administered P301S/E4 mice. Collectively, these findings suggest that the inhibition of OXR signaling through lembor exant may confer neuroprotection, distinct from general sleep-promoting effects.

OXR antagonism ameliorates chronic glial reactivity

Given prior findings from our lab and others that microglia are required for tau-mediated neurodegeneration in P301S mice^{27,29,30,32}, we hypothesized that the marked reduction in brain atrophy in lemborexant-treated male mice was linked with reduced microglial reactivity, which may potentially serve as a mechanism in preventing neuronal damage led by chronic inflammation. To address this hypothesis, we immunohistochemically quantified markers of reactive microglia across the spectrum of disease-associated or homeostatic populations^{33,34} in both

hippocampus and entorhinal/piriform cortex and noticed substantial changes in the lemborexant-treated groups, especially in the entorhinal/piriform cortex (Fig. 3). Indeed, we observed a signficant reduction in ionized calcium-binding adaptor molecule 1 (Iba1) by -50% in the lemborexant-treated group at ZT13 and -30% in lemborexant-treated groups at ZT3 compared to the vehicle group. The zolpidem-treated group showed no substantial changes relative to the controls, suggesting an overall reduction in reactive microglial population due to OXR antagonism. Furthermore, disease-associated microglial markers such as Clec7a (Fig. 3a,c,g) and Cd68 (Fig. 3a,e,i), a marker of phagolysosomal activity, were decreased in the lemborexant-treated mice, more prominently in the ZT13 group relative to vehicle-administered P301S/E4 male mice. In line with this, we observed a significant increase in Tmem119, a homeostatic microglial marker in P301S/E4 mice treated with lemborexant (Fig. 3a,d,h). These data suggest that the effect of

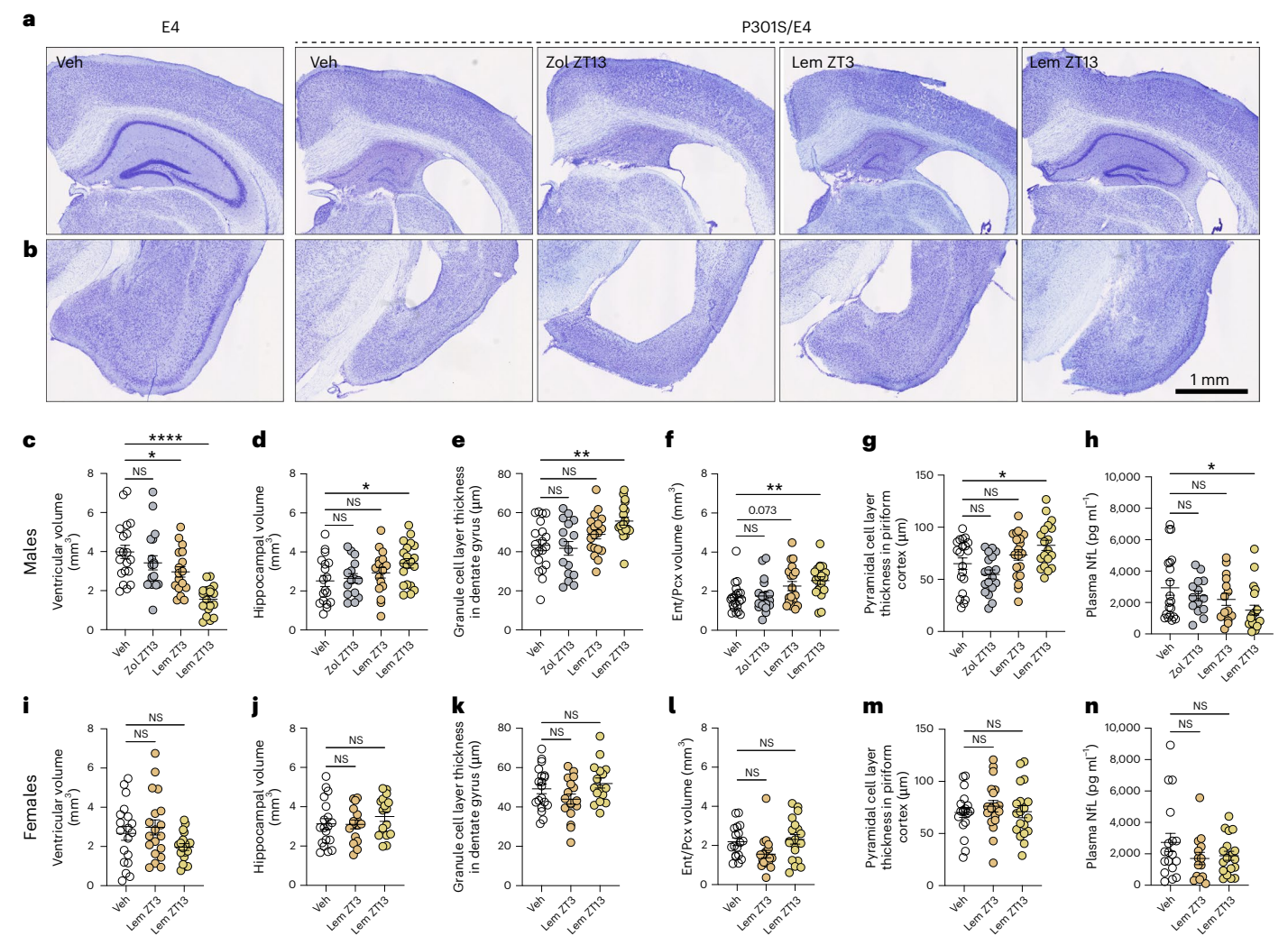


Fig. 2| **OXR** antagonism is partially neuroprotective in P3015/E4 mice. **a,b**, Representative images of cresyl violet-stained male mouse hippocampal (**a**) and Ent/Pcx cortex for volumetric analysis (**b**). Using male mice—**c**, ventricular volume ($n_{\text{Veh}} = 20, n_{\text{ZoI}ZT13} = 18, n_{\text{Lem}ZT3} = 18, n_{\text{Lem}ZT3} = 20$; one-way ANOVA, Dunnett's post hoc test); **d**, hippocampal volume ($n_{\text{Veh}} = 18, n_{\text{ZoI}ZT13} = 15, n_{\text{Lem}ZT3} = 17, n_{\text{Lem}ZT13} = 20$, one-way ANOVA, Dunnett's post hoc test); **e**, granule cell layer thickness in dentate gyrus ($n_{\text{Veh}} = 20, n_{\text{ZoI}ZT13} = 16, n_{\text{Lem}ZT3} = 19, n_{\text{Lem}ZT13} = 19$; one-way ANOVA, Dunnett's post hoc test); **e**, one-way ANOVA, Dunnett's post hoc test); **g**, pyramidal cell layer thickness in piriform cortex ($n_{\text{Veh}} = 20, n_{\text{ZoI}ZT13} = 18, n_{\text{Lem}ZT13} = 19$; one-way ANOVA, Dunnett's post hoc test); **g**, pyramidal cell layer thickness in piriform cortex ($n_{\text{Veh}} = 20, n_{\text{ZoI}ZT13} = 18, n_{\text{Lem}ZT13} = 19$; one-way ANOVA, Dunnett's post hoc test); **h**, quantification of plasma NfL levels measured by SIMOA ($n_{\text{Veh}} = 20, n_{\text{ZoI}ZT13} = 14, n_{\text{Lem}ZT13} = 15, n_{\text{Lem}ZT13} = 20$; Kruskal-Wallis test and Dunn's post hoc test). Using

female mice—**i**, ventricular volume ($n_{\text{Veh}} = 19, n_{\text{LemZTI3}} = 19, n_{\text{LemZTI3}} = 19$; one-way ANOVA, Dunnett's post hoc test); **j**, hippocampal volume ($n_{\text{Veh}} = 19, n_{\text{LemZTI3}} = 16$; $n_{\text{LemZTI3}} = 17$; one-way ANOVA, Dunnett's post hoc test); **k**, granule cell layer thickness in dentate gyrus ($n_{\text{Veh}} = 19, n_{\text{LemZTI3}} = 17, n_{\text{LemZTI3}} = 16$; one-way ANOVA, Dunnett's post hoc test); **l**, Ent/Pcx volume ($n_{\text{Veh}} = 18, n_{\text{LemZTI3}} = 20, n_{\text{LemZTI3}} = 20$; one-way ANOVA, Dunnett's post hoc test); **m**, pyramidal cell layer thickness in piriform cortex ($n_{\text{all}} = 19$; one-way ANOVA, Dunnett's post hoc test); **n**, quantification of plasma NfL levels measured by SIMOA ($n_{\text{Veh}} = 18, n_{\text{LemZTI3}} = 14, n_{\text{LemZTI3}} = 18$; Kruskal—Wallis test and Dunn's post hoc test). For detailed statistical information, see Supplementary Table 1. Data represent mean \pm s.e.m. of biological replicates; *P < 0.05, **P < 0.01 and ****P < 0.0001. Ent/Pcx, entorhinal/piriform.

lemborexant on modulating neurodegeneration may involve mitigating a disease-associated reactive microglial state. This is further supported by our finding that in lemborexant-treated P301S/E4 mice, both astroglial and microglial ApoE colocalization were significantly reduced (Fig. 3j-m) by -50%, the latter of which is more commonly observed during elevated inflammatory and damaging conditions. We initially hypothesized that blocking orexin signaling may directly influence microglia to mitigate neurodegeneration. However, we found no significant changes in glial reactivity in lemborexant-treated E4 mice without tau pathology (Extended Data Fig. 1b-f), despite a similar increase in NREM sleep (Extended Data Fig. 1a). Overall, these findings suggest that while blocking orexin signaling is effective in averting chronic inflammation compared to zolpidem-mediated GABA_A agonism or vehicle-administered P301S/E4 male mice, the mechanism

of action responsible likely does not involve a direct modulation of orexin signaling on glia.

Lemborexant prevents synapse degeneration

To gain insights into potential mechanisms behind the observed changes in microglial reactivity and neurodegeneration by lemborexant-induced NREM sleep, we performed RNA sequencing (RNA-seq) in bulk tissue and found gene expression changes involved in multiple functional modalities including hormonal and GPCR ligand binding, glial cell differentiation, synaptic modulation, particularly of excitatory synapses, and response to DNA damage (Fig. 4a,b). We primarily compared P301S/E4 male mice administered with vehicle to lemborexant-treated group at ZT13, as this group displayed the most prominent pathological changes. Genes involved in glial cell

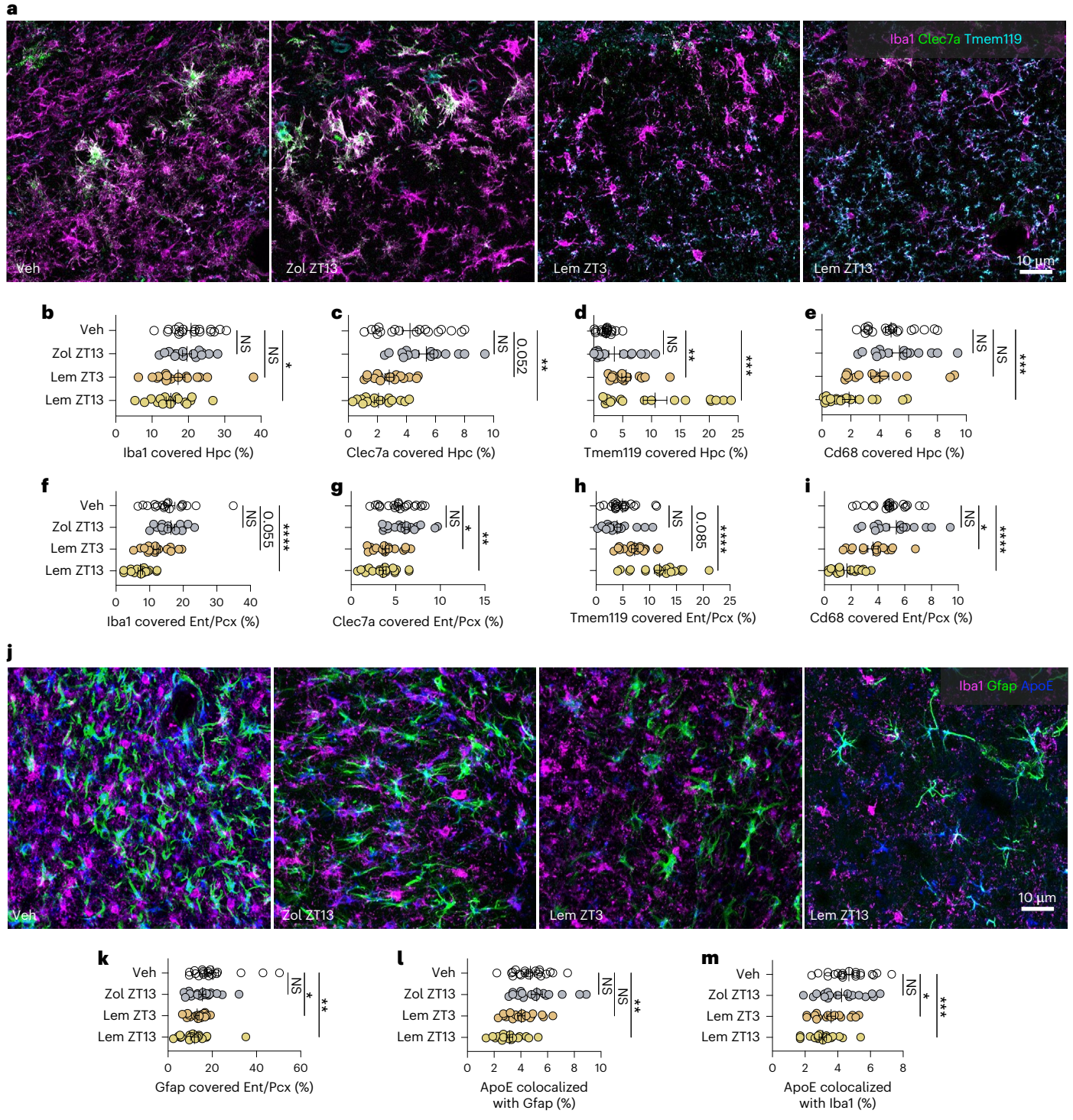


Fig. 3 | **Blocking OXR signaling alters microglial reactivity in male P301S/E4 mice. a**, Representative images of lba1 (magenta), Clec7a (green) and Tmem119 (cyan) costained microglia in the Ent/Pcx in male P301S/E4 mice. Scale bar, 10 μm. **b**, Quantification of percentage lba1 ($n_{\text{Veh}} = 18$, $n_{\text{ZoIZTI3}} = 15$, $n_{\text{Lem ZTI3}} = 16$, $n_{\text{Lem ZTI3}} = 17$; one-way ANOVA and Dunnett's post hoc test). **c**, Quantification of percentage Clec7a ($n_{\text{Veh}} = 18$, $n_{\text{ZoIZTI3}} = 15$, $n_{\text{Lem ZTI3}} = 16$; one-way ANOVA and Dunnett's post hoc test). **d**, Quantification of percentage Tmem119 ($n_{\text{Veh}} = 18$, $n_{\text{ZoIZTI3}} = 15$, $n_{\text{Lem ZTI3}} = 15$, $n_{\text{Lem ZTI3}} = 17$; one-way ANOVA and Dunnett's post hoc test. **e**, Quantification of percentage Cd68 ($n_{\text{Veh}} = 19$, $n_{\text{ZoIZTI3}} = 15$, $n_{\text{Lem ZTI3}} =$

Dunnett's post hoc test). **h**, Quantification of percentage Tmem119 ($n_{\rm Veh}$ = 20, $n_{\rm ZoIZTI3}$ = 19, $n_{\rm LemZTI3}$ = 17, $n_{\rm LemZTI3}$ = 19; one-way ANOVA and Dunnett's post hoc test). **i**, Quantification of percentage Cd68 ($n_{\rm Veh}$ = 20, $n_{\rm ZoIZTI3}$ = 15, $n_{\rm LemZTI3}$ = 15, $n_{\rm LemZTI3}$ = 19; one-way ANOVA and Dunnett's post hoc test) covered Ent/Pcx in Veh-, Zol- and Lem-treated mice. **j**, Representative images of Iba1 (magenta), Gfap (green) and ApoE (blue) costained glia in the Ent/Pcx. **k**, Quantification of percentage Gfap covered Ent/Pcx ($n_{\rm Veh}$ = 19, $n_{\rm ZoIZTI3}$ = 18, $n_{\rm LemZTI3}$ = 18, $n_{\rm LemZTI3}$ = 18; one-way ANOVA and Dunnett's post hoc test. **l**, Quantification of percentage ApoE colocalized with Gfap ($n_{\rm Veh}$ = 19, $n_{\rm ZoIZTI3}$ = 17, $n_{\rm LemZTI3}$ = 18, $n_{\rm LemZTI3}$ = 18; one-way ANOVA and Dunnett's post hoc test). **m**, Quantification of percentage ApoE colocalized with Iba1 ($n_{\rm Veh}$ = 19, $n_{\rm ZoIZTI3}$ = 17, $n_{\rm LemZTI3}$ = 16, $n_{\rm LemZTI3}$ = 18; one-way ANOVA and Dunnett's post hoc test) in Ent/Pcx. For detailed statistical information, see Supplementary Table 1. Data represent mean \pm s.e.m. of biological replicates; *P< 0.005, **P< 0.001 and ****P< 0.0001. Hpc, hippocampus.

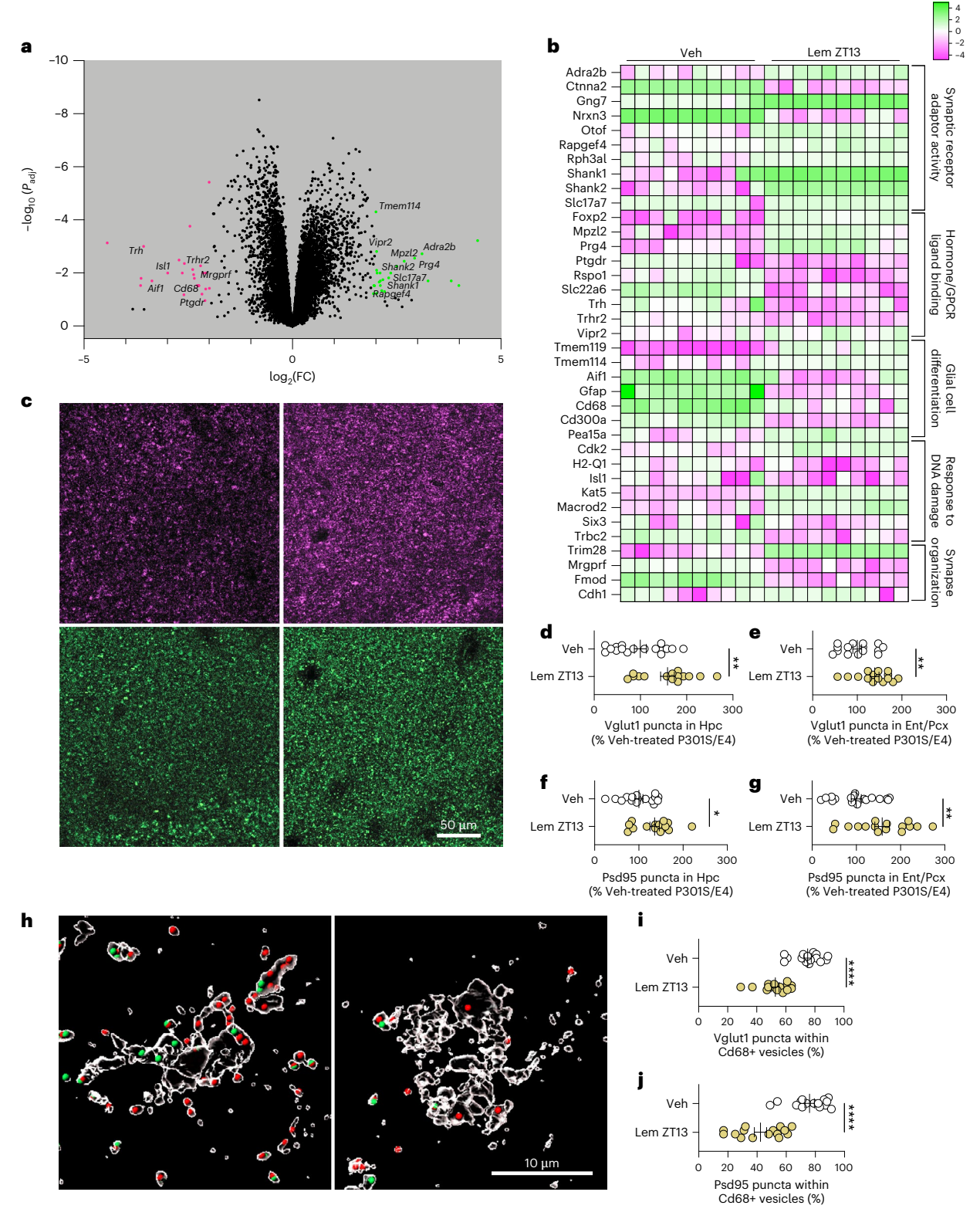


Fig. 4 | **Lemborexant alters synaptic receptor and GPCR ligand binding activity pathways. a**, Volcano plot comparing differentially regulated genes in P301S/E4 male mice treated with control Veh compared to Lem at ZT13. Cut-off value for significance is set at twofold log(FC). **b**, Heatmap of P301S/E4 Veh versus Lem ZT13 mice that reached significance of adjusted P < 0.05 grouped by gene ontology terms (n = 10 mice per treatment group). **c**, Representative images of presynaptic Vglut1 (magenta) and postsynaptic Psd95 stained (green) in Ent/Pcx in male P301S/E4 mice quantified in **e**. **d**, Percentage Vglut1 puncta quantified in Hpc ($n_{\text{Veh}} = 18$, $n_{\text{Lem}ZT13} = 15$; two-tailed t test); **e**, Ent/Pcx ($n_{\text{Veh}} = 15$, $n_{\text{Lem}ZT13} = 15$; two-tailed t test). **f**, Percentage of Psd95 puncta quantified in Hpc ($n_{\text{Veh}} = 18$,

 $n_{\mathrm{Lem}ZT13}$ = 15, two-tailed t test). \mathbf{g} , Ent/Pcx cortex (n_{Veh} = 18, $n_{\mathrm{Lem}ZT13}$ = 15; two-tailed t test). \mathbf{h} , Three-dimensional reconstructed representative images of Vglut1 (red) and Psd95 (green) synaptic engulfment within Cd68 (white) phagolysosomes in Veh and Lem ZT13 male P301S/E4 mice. \mathbf{i} , Percentage of Vglut1 puncta (n = 15 mice per group; two-tailed t test). \mathbf{j} , Percentage of Psd95 puncta within Cd68* vesicles (n = 15 mice per group; two-tailed t test) quantified in male P301S/E4 mice treated with Veh or Lem ZT13. For detailed statistical information, see Supplementary Table 1. Data represent mean \pm s.e.m. of biological replicates; *P < 0.05, **P < 0.01 and ****P < 0.0001. FC, fold change.

differentiation, including Tmem119, Tmem114, Cd68, Aif1, Cd300a, Pea15a and H2-O1, were all differentially decreased in mice treated with lemborexant at ZT13 (Fig. 4a,b), consistent with a reduced microglial response to the pathological changes after treatment-related amelioration (Figs. 1 and 2). Interestingly, a large majority of differentially regulated genes involved GPCR signaling and synaptic modulation, notably Foxp2, Rapgef4, Ptgdr, Rspo1, Slc17a7, Shank1 and Shank2. A comparable increase was validated by immunohistochemical quantification of presynaptic vesicular glutamate transporter (Vglut1; Slc17a7) and postsynaptic density markers (Psd95; Shank1 and Shank2; Fig. 4c-g), supporting the finding that blocking orexin-mediated excitatory GPCR signaling^{16,17} using lemborexant preserves synaptic integrity, as evidenced by substantial conservation of synaptic puncta in both hippocampus and entorhinal/piriform cortex. In addition, we found lemborexant treatment prevented excessive microglial engulfment of synapses, marked by reduced Vglut1+ and Psd95+ neuronal synaptic puncta within Cd68⁺ phagolysosomes (Fig. 4h-j). These findings further support the link between a reduction in chronic inflammation and synaptic damage, potentially contributing to neuroprotection.

Lemborexant reduces PKA-mediated phosphorylation of tau in male mice

Given that synaptic and neuronal activity directly influences the release of tau protein^{35,36}, which affects tau pathology and its propagation in vivo^{36,37}, we aimed to investigate whether the observed pathological changes, including a reduction in brain atrophy after blocking OXR signaling, were attributed to alterations in pathological tau. We performed immunohistochemical analyses using antibodies that specifically recognize tau at various disease-associated phosphorylation sites and found a reduction in AT8⁺ (Ser202 and Thr205; Fig. 5a-c) as well as PG5⁺ (Ser409; Fig. 5d-f) pTau in lemborexant-treated male mice with minimal changes in zolpidem-treated mice compared to controls. We also found reduced accumulation of MC1+ (confirmation-dependent tau epitope; Fig. 5g-i) aggregated tau deposits. Consistent with pathological changes in brain atrophy and glial reactivity, the lemborexant-treated group at ZT13 exhibited a greater reduction in pathological tau compared to other treatment groups, with a ~50% decrease compared to vehicle, while the lemborexant-treated group at ZT3 showed a 30-40% reduction. Interestingly, both lemborexant groups demonstrated a stronger response in preventing tau phosphorylated at Ser409 compared to Ser202 and Thr205, hinting at the possibility that blocking orexin signaling might be more effective in modulating specific pTau species.

Binding to OXR1 and OXR2 triggers nonselective cation channels or phosphorylation of phospholipases (PL) and protein kinases (PK) to facilitate excitatory neurotransmission. These include PKC and PKA, which are known to abnormally hyperphosphorylate tau, leading to mechanisms that increase the propensity of tau to aggregate, which over time lead to neuronal death. In fact, the PG5 antibody selectively recognizes PKA-dependent phosphorylation of tau. We explored whether the changes in pTau due to OXR antagonism were associated with alterations in the PLC/PKC and adenylyl cyclase (AC)/PKA pathways along with phosphorylation of their downstream effectors such as extracellular signal regulated kinase (ERK) and p38 mitogen-activated protein kinase (MAPK) (Fig. 6). First, we tested the signaling pathways affected by lemborexant-mediated OXR antagonism by measuring secondary messengers diacylglycerol (DAG) and cyclic adenosine monophosphate (cAMP) produced upon PLC and AC activation, respectively. We found a significant reduction in DAG levels in males treated with lemborexant at ZT3 with minimal changes in the lemborexant-treated male group at ZT13 compared to vehicle (Fig. 6a). In contrast, cAMP levels were reduced in both lemborexant treatment groups compared to vehicle. As expected, zol ZT13 mice showed no signficant changes in DAG and cAMP. Lemborexant-treated female mice that showed no improvements in regional atrophy displayed a significant reduction in DAG, with negligible changes in cAMP levels (Extended Data Fig. 3a.b). These data support a potential GPCR-mediated signaling modulation on pTau and associated neurodegeneration in males. In line with this, immunoblotting for proteins involved in the PLC/PKC and AC/PKA pathways revealed a dramatic reduction in phosphorylated PKA, ERK and p38 in the lemborexant-treated male groups only, compared to vehicle (Fig. 6c-g). A similar reduction was not observed in phosphorylated PKC in males or any of the cell signaling molecules in the female mice (Extended Data Fig. 3c-g). Because the male group treated with lemborexant at ZT13 consistently demonstrated a stronger response across all measures, we examined whether the expression of OXRs, kinases and cell signaling molecules involved in tau phosphorylation was influenced by circadian rhythms. We did not observe any gene expression differences between ZT3 and ZT13 (Extended Data Fig. 4a-i). Similarly, we found no differences across treatment groups (Extended Data Fig. 4j-r). While we cannot exclude potential cross-talk between the PKA and other cell signaling pathways, the data so far suggest that blocking orexin signaling in males reduces PKA-mediated phosphorylation of tau. In further support of this, we found significant reductions in PHFs (PHF1) tau in lemborexant-treated males at both timepoints (Fig. 6c,h), which requires PKA-mediated phosphorylation in its early development³⁸.

OXR2 knockout prevents tau seeding and propagation

While lembor exant interacts with both OXR1 and OXR2, it preferentially binds to OXR2 (ref. 39). To genetically validate the observed reduction in pTau after lemborexant treatment, we investigated the effects on tau seeding and spreading in OXR2^{KO} mice (Fig. 7). Briefly, we experimentally induced tau seeding in a prion-like manner by intrahippocampally injecting AD-tau-enriched homogenate⁴⁰ in nontau, male OXR2WT and OXR2^{KO} mice at 7 months of age (Fig. 7a). In addition, we included a separate group of experimentally seeded OXR2WT mice that were treated with lemborexant (OXR2WTLem) starting from 7.5 months to 9.5 months at ZT13. Two weeks after inoculation, we measured their sleep-wake behavior using Piezosleep sensor pads instead of electroencephalography (EEG) to avoid additional cerebral surgeries. We observed a striking similarity in sleep pattern between OXR2 $^{\! \scriptscriptstyle WT\, Lem}$ and OXR2 $^{\! \scriptscriptstyle KO}$ mice at baseline (Extended Data Fig. 5a). This effect appeared to be largely driven by a reduction in wake bout length time during the dark phase compared to OXR2^{WT} mice. Measuring sleep-wake behavior at 9.5 months showed a similar, nearly 75%, increase in percentage sleep in OXR2WT Lem and OXR2KO mice during the dark phase compared to OXR2WT mice (Extended Data Fig. 5b). The OXR2KO mice displayed significant changes in sleep bout length in both the light and dark phases, suggesting fragmented sleep, unlike OXR2WTLem mice (Extended Data Fig. 5b). In OXR2WTLem mice, sleep bout length increased only during the dark phase, corresponding to a reduction in wake bout length following gavage. While the percentage of sleep during the dark phase reduced over 2 months in OXR2^{WT} mice, both OXR2^{WT Lem} and OXR2^{KO} mice showed minimal changes (Extended Data Fig. 5c). Furthermore, an approximate 20% increase in wake bout length in the dark phase was $quantified \, over \, 2 \, months, while \, OXR2^{WTLem} \, and \, OXR2^{KO} \, mice \, displayed \, a \, months \, and \, oxresh \, and$ 40% decrease and a marginal 7% increase, respectively. These data suggest that genetic and pharmacological manipulation of OXR2 display similar sleep-wake patterns, with diminished decline in sleep over time.

In line with this, both OXR2^{WT Lem} and OXR2^{KO} mice displayed a significant reduction in AT8 and PG5⁺ seeding of pathological tau in the hippocampus compared to OXR2^{WT} mice (Fig. 7b-e). This reduction corresponded with decreased propagation of PG5⁺ pTau at 1 mm anterior and posterior hippocampus to the injection site (Extended Data Fig. 5e-g), with the most noticeable changes observed in the dentate gyrus and CA3, respectively. Although we did not observe a significant anterior spread of AT8⁺ pTau, there was a notable decrease in tau propagation in the posterior hippocampus compared to OXR2^{WT}

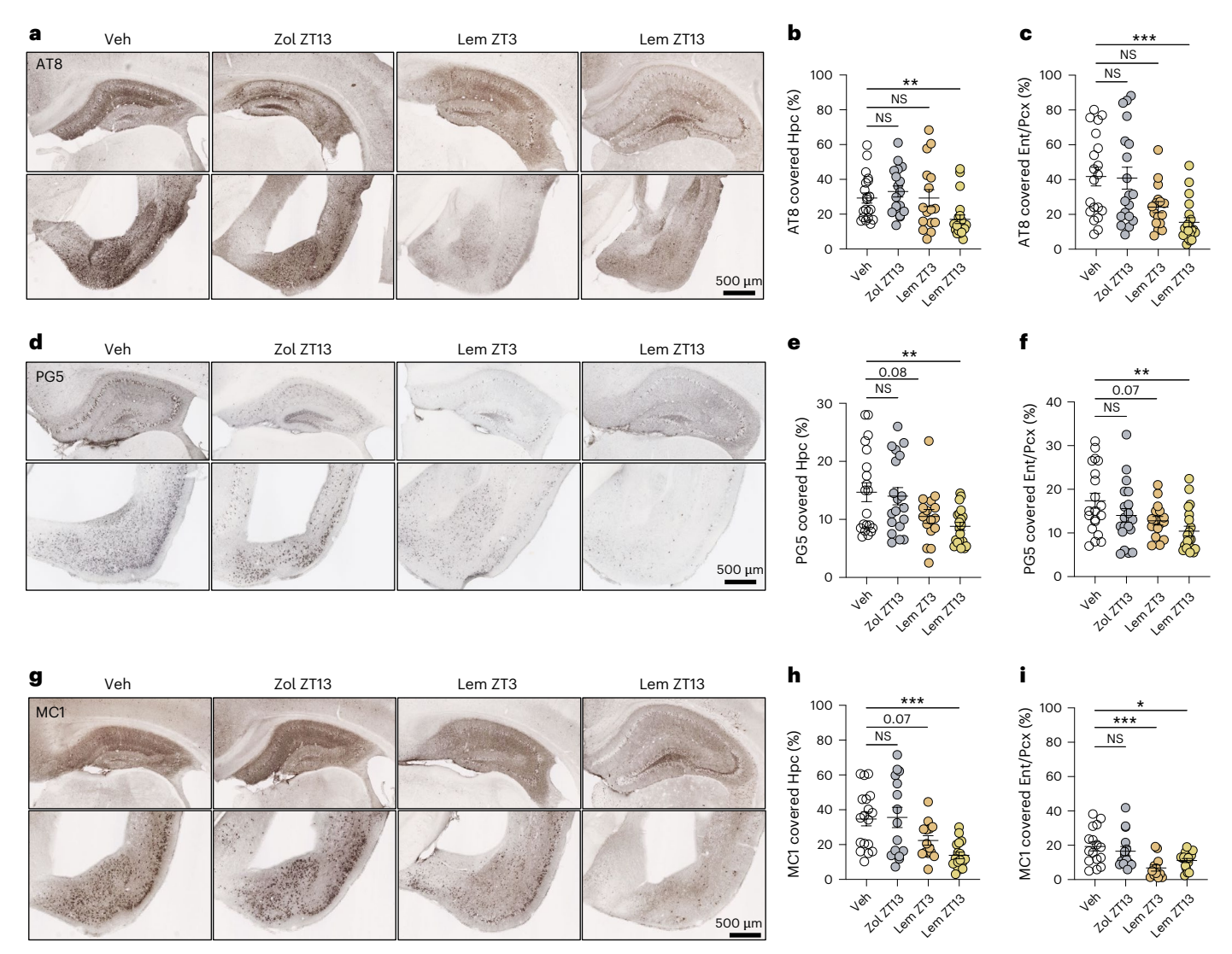


Fig. 5 | **Lemborexant treatment reduces hyperphosphorylated pathological tau in male P301S/E4 mice. a**, Representative images of AT8-stained pTau at both serine 202 and threonine 205. Top: Hpc. Bottom: Ent/Pcx. **b**, Quantification of percentage AT8-covered Hpc ($n_{\text{Veh}} = 20$, $n_{\text{ZoIZTI3}} = 18$, $n_{\text{LemZTI3}} = 16$, $n_{\text{LemZTI3}} = 20$; Kruskal–Wallis test and Dunn's post hoc test). **c**, Quantification of percentage AT8-covered Ent/Pcx ($n_{\text{Veh}} = 20$, $n_{\text{ZoIZTI3}} = 19$, $n_{\text{LemZTI3}} = 16$, $n_{\text{LemZTI3}} = 20$; Kruskal–Wallis test and Dunn's post hoc test. **d**, Representative images of PG5-stained pTau at serine 409. **e**, Quantification of percentage PG5-covered Hpc ($n_{\text{Veh}} = 20$, $n_{\text{ZoIZTI3}} = 19$, $n_{\text{LemZTI3}} = 16$, $n_{\text{LemZTI3}} = 20$; one-way ANOVA and Dunnett's post

hoc test). **f**, Quantification of percentage PG5-covered Ent/Pcx (n_{Veh} = 20, $n_{Z\text{o}|ZT13}$ = 20, $n_{\text{Lem}ZT3}$ = 16, $n_{\text{Lem}ZT13}$ = 20; one-way ANOVA and Dunnett's post hoc test). **g**, Representative images of MC1* aggregated tau in Hpc and Ent/Pcx. **h**, Percentage MC1 covered Hpc (n_{Veh} = 18, $n_{Z\text{o}|ZT13}$ = 15, $n_{\text{Lem}ZT3}$ = 14, $n_{\text{Lem}ZT13}$ = 17; one-way ANOVA and Dunnett's post hoc test). **i**, Percentage MC1 covered Ent/Pcx (n_{Veh} = 16, $n_{Z\text{o}|ZT13}$ = 15, $n_{\text{Lem}ZT3}$ = 12, $n_{\text{Lem}ZT13}$ = 17; one-way ANOVA and Dunnett's post hoc test). For detailed statistical information, see Supplementary Table 1. Data represent mean \pm s.e.m. of biological replicates; *P < 0.05, **P < 0.01 and ***P < 0.001.

mice (Extended Data Fig. 5h–j). In line with previous findings (Fig. 6), we detected no changes in DAG levels in either group, while cAMP concentrations were reduced by approximately 20% in OXR2 $^{\rm WTLem}$ and OXR2 $^{\rm KO}$ mice, compared to OXR2 $^{\rm WT}$ mice (Fig. 7f,g). This was further supported by a reduction in phosphorylated PKA and PHF, with no significant changes in phosphorylated PKC (Fig. 7h), suggesting that the reduction in tau seeding and propagation may result from a diminished AC/cAMP/PKA pathway in mice lacking OXR signaling.

Discussion

OXRs are clinically approved targets for the treatment of sleep disorders, although a direct link between OXR inhibition and tau-mediated neurodegeneration has not yet been assessed. Our lab and others have previously shown that tau aggregation and deposition, especially in the key sleep—wake centers, contribute to diminished REM and NREM sleep as well as pronounced hyperarousal in tau transgenic mice compared

to wild-type mice 9,31 . Similar changes in sleep—wake cycle have been reported in human tauopathy 41,42 . In our study, we present new evidence that lemborexant-mediated changes in sleep—wake behavior with decreased OXR signaling are neuroprotective in P301S/E4 male mice. In support of this, we found that lemborexant treatment mitigated neuronal and synaptic damage, most likely due to its effects on suppressing detrimental pTau as well as preventing chronic neuroinflammation. In contrast, the nonorexinergic GABA_a agonist zolpidem that evoked a similar acute response to NREM sleep, although for a shorter duration than lemborexant, did not produce these protective effects. These findings support the likelihood that preventing neurodegeneration necessitates OXR antagonism rather than a general increase in NREM sleep.

In terms of the effects on sleep, tau and neurodegeneration, we consistently observed a stronger response in the P301S/E4 mice treated with lembor exant at ZT13 compared to the ZT3 group. We ruled out

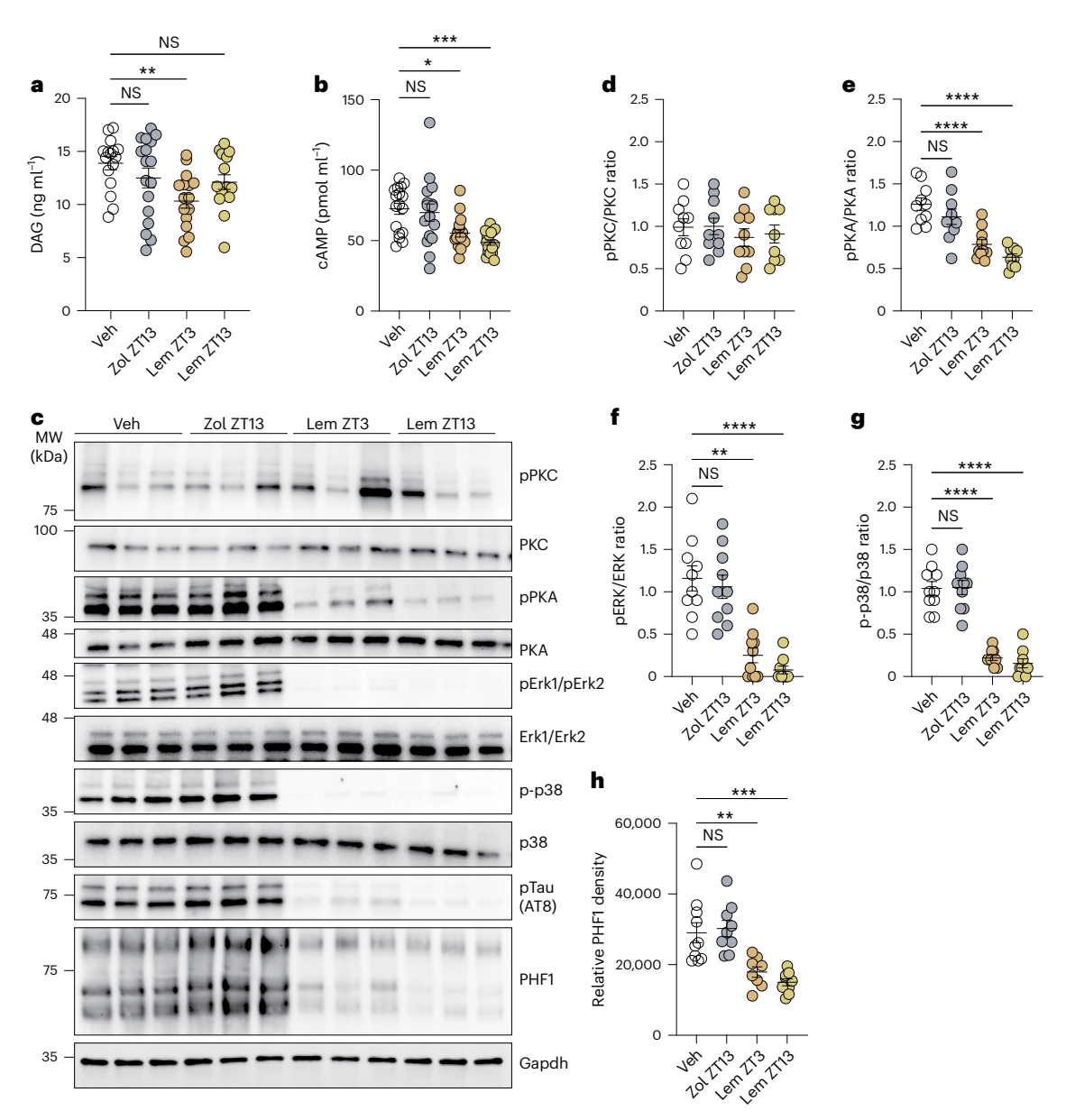


Fig. 6 | OXR antagonism reduces cAMP/PKA-mediated phosphorylation of tau in P301S/E4 male mice. a, DAG ($n_{\rm veh}=16,n_{\rm ZoIZTI3}=17,n_{\rm LemZTI3}=16$, $n_{\rm LemZTI3}=15$; one-way ANOVA and Dunnett's post hoc test). b, cAMP ELISAS ($n_{\rm Veh}=17,n_{\rm ZoIZTI3}=16,n_{\rm LemZTI3}=17,n_{\rm LemZTI3}=17$; Kruskal–Wallis test and Dunn's post hoc test) of RIPA-soluble Ent/Pcx extracts from Veh controls, Zol- and Lem-treated mice. c, Immunoblots of RIPA-soluble Ent/Pcx brain extracts from Veh-, Zol- and Lem-treated male mice (n=3 mice per group; one-way ANOVA and Dunnett's post hoc test). d–h, Quantification of the western blot intensity of PK and cell signaling proteins (for all quantifications except PHF1- $n_{\rm Veh}=10$,

 $n_{\rm ZoIZT13}$ = 10, $n_{\rm Lem ZT3}$ = 10, $n_{\rm Lem ZT13}$ = 9; for PHF1- $n_{\rm Veh}$ = 10, $n_{\rm ZoIZT13}$ = 9, $n_{\rm Lem ZT3}$ = 8, $n_{\rm Lem ZT13}$ = 9). All proteins were first normalized to Gapdh, and the ratio of phosphorylated to their corresponding unphosphorylated form was then calculated. PHF1 was normalized to Gapdh (**d**—one-way ANOVA and Dunnett's post hoc test; **e**—one-way ANOVA and Dunnett's post hoc test; **f**—Kruskal–Wallis test and Dunn's post hoc test; **g**—one-way ANOVA and Dunnett's post hoc test; **h**—one-way ANOVA; P < 0.0001; Dunnett's post hoc test). For detailed statistical information, see Supplementary Table 1. Data represent mean \pm s.e.m. of biological replicates; *P < 0.05, **P < 0.01, ***P < 0.001 and ****P < 0.0001.

circadian influences on OXRs and associated secondary messengers or kinases by confirming that their expression levels were similar at both ZT3 and ZT13. Thus, our findings suggest that blocking orexin signaling and increasing NREM sleep, in addition to reducing total wake, are most effective at preventing tau-mediated neurodegeneration. A similar positive effect on improving sleep architecture with zolpidem and an OXR2-selective antagonist has recently been reported, demonstrating reduced wake periods during the active phase in another tau transgenic mouse model 31,43. Interestingly, the authors also noted sex differences in response to the OXR2-selective antagonist, observing no effect in females. It is plausible that the effects of OXR antagonism were less pronounced in females, given that female mice show less regional brain

atrophy than males of the same age. In our study, we speculate that the observed effect in males may stem from inherent physiological differences in tau pathology as well as downstream molecular responses triggered by lemborexant-mediated OXR antagonism, despite a similar effect on sleep—wake behavior. The consistent findings across two different tau transgenic models using two distinct OXR antagonists underscore the importance of assessing the therapeutic efficacy of blocking OXR signaling in both sexes.

Reactive microglia are critical modulators of neuronal and synaptic damage, acting as both protectors and potential contributors to neurodegeneration in P301S mice^{29,30,44}. In line with the reduced brain atrophy, a reduction in reactive microgliosis was only observed in

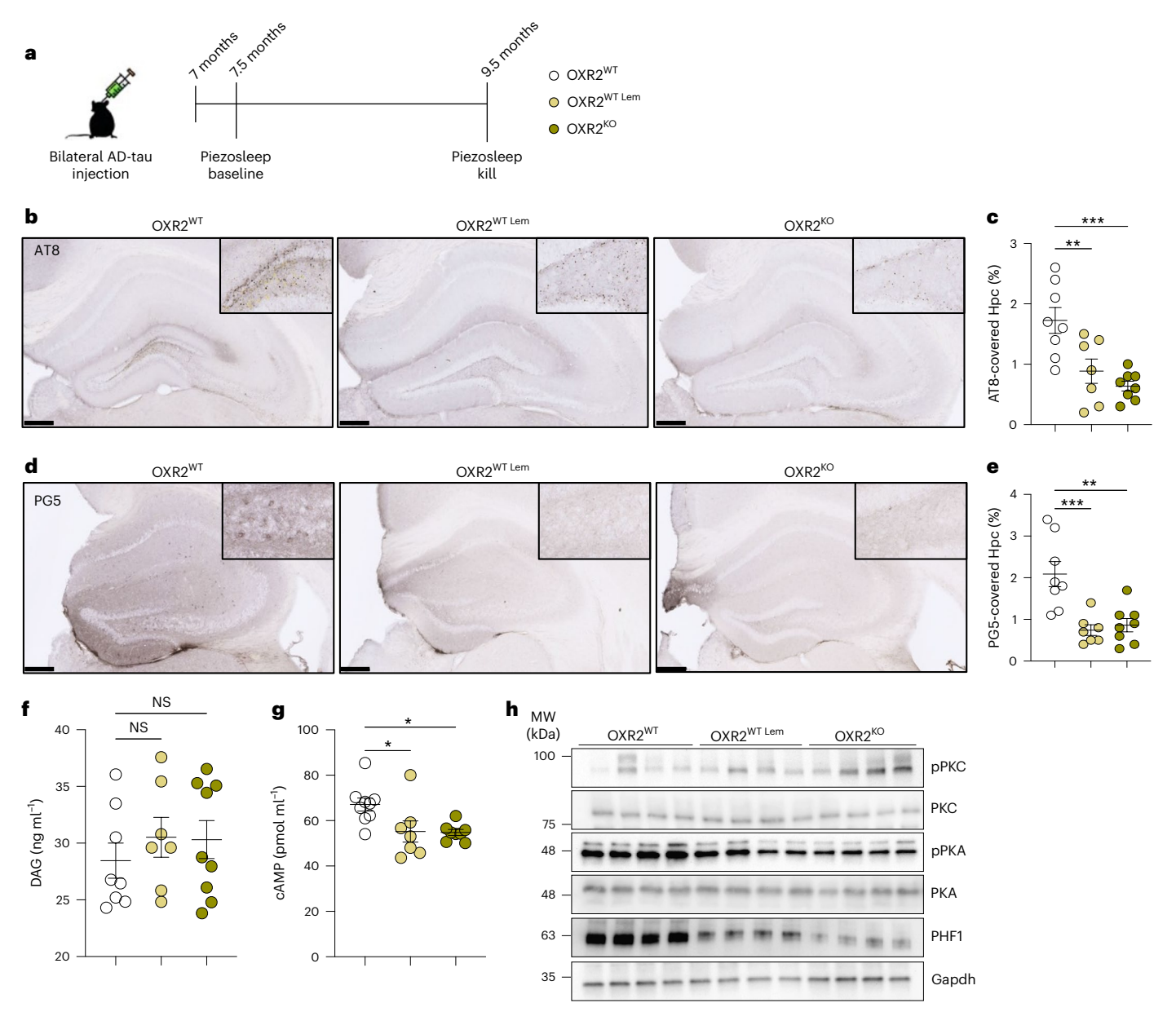


Fig. 7 | **Pharmacological or genetic lack of OXR signaling decreases tau seeding and cAMP/PKA-mediated phosphorylation of tau. a**, Schematic illustration of study design. **b**, Representative AT8-stained images from AD-tau-injected OXR2^{WT} mice (controls), OXR2^{WT} mice treated with Lem at ZT13 and OXR2^{KO} mice. **c**, Percentage AT8 stain quantified in Hpc ($n_{\text{OXR2-WT}} = 8$, $n_{\text{OXR2-WT-Lem}} = 7$, $n^{\text{OXR2-KO}} = 8$; one-way ANOVA and Dunnett's post hoc test). **d**, Representative PG5-stained images from AD-tau-injected OXR2^{WT} mice, OXR2^{WT} mice treated with Lem at ZT13 and OXR2^{KO} mice. **e**, Percentage PG5 stain quantified in Hpc ($n_{\text{OXR2-WT}} = 8$,

$$\begin{split} &n_{\text{OXR2-WTLem}} = 7, n_{\text{OXR2-KO}} = 8; \text{ one-way ANOVA and Dunnett's post hoc test)}. \textbf{f}, \text{DAG} \\ &(n_{\text{OXR2-WTLem}} = 7, n_{\text{OXR2-KO}} = 9; \text{ one-way ANOVA and Dunnett's post hoc test)}; \textbf{g}, \text{cAMP} (n_{\text{OXR2-WTLem}} = 7, n_{\text{OXR2-WTLem}} = 7, n_{\text{OXR2-KO}} = 8; \text{ one-way ANOVA}; P = 0.0125; \\ \text{Dunnett's post hoc test)} \text{ ELISAs of RIPA-soluble Hpc extracts.} \textbf{h}, \text{ Immunoblots of RIPA-soluble Hpc brain extract from AD-tau-injected OXR2}^{\text{WT}} \text{ mice, OXR2}^{\text{WT}} \\ \text{mice treated with Lem at ZT13 and OXR2}^{\text{KO}} \text{ mice } (n = 4 \text{ mice per treatment group)}. \\ \text{For detailed statistical information, see Supplementary Table 1. Data represent mean \pm s.e.m. of biological replicates; *P < 0.05, **P < 0.01 and ***P < 0.001.} \end{split}$$

lemborexant-treated compared to vehicle- or zolpidem-administered P301S/E4 male mice. To this end, an important question to resolve is whether the neuroprotective effects of lemborexant were observed due to decreased reactive microglial-mediated damage, increased microglial phagocytosis of tau or as a consequence of reduction in pTau pathology. We found no changes in reactive microglial markers in E4 mice that do not overexpress P301S tau, indicating that a pre-existing inflammatory trigger may be required to observe a microglial response to lemborexant. Indeed, we found an overall reduction in pro-inflammatory reactive microglia markers such as Clec7a and Cd68 in P301S/E4 mice, with a concomitant increase in homeostatic microglia such as Tmem119. Microglial phagocytosis of proteopathic

aggregates, including tau, is typically associated with upregulated Cd68, which contrasts with what we observed. In line with this, microglial phagolysosomal engulfment of presynaptic and postsynaptic boutons was also reduced. In addition, our RNA-seq data did not reveal differential expression of CLEAR genes found with amplified microglial engulfment of tau⁴⁴. The degree of ApoE colocalization with lba1⁺ microglia was relatively lower in lemborexant-treated mice compared to zolpidem- or vehicle-administered mice, suggesting less inflammatory damage. Furthermore, the vast majority of OXRs are expressed in neurons⁴⁵. Taken together, the evidence does not support the notion that lemborexant directly acts on microglia to reduce reactive microglia-mediated damage or enhances the phagocytic uptake

or clearance of tau. However, an indirect effect cannot be excluded, as OXR signaling influences various neurotransmitters, including noradrenaline, which is known to impact microglial surveillance $^{46,47}-$ a characteristic of a more homeostatic microglial state. Supporting this, we identified a downregulation of Adra2b, which encodes the $\alpha\text{-}2B$ adrenergic receptor, a GPCR that inhibits noradrenaline availability 48 . Additionally, we observed an increase in thyrotropin-releasing hormone (Trh) and its receptor (Trhr2), a GPCR involved in behavioral arousal, partly mediated by orexin. Notably, reduced Trhr signaling has been shown to elevate noradrenaline release 49 . These findings indicate that modulating orexin signaling may indirectly influence factors such as noradrenaline, contributing to the more homeostatic microglial profile observed in the lemborexant-treated groups.

OXRs are classified as promiscuous GPCRs, capable of signaling through G proteins from at least three distinct subfamilies. While such versatility is typical for GPCRs, the mechanisms determining which G proteins are activated by OXRs in specific tissues remain poorly understood. Furthermore, there is no definitive evidence distinguishing unique signaling pathways for the two OXR subtypes. However, it is established that OXR activation influences downstream effectors such as PL, ion channels and PK, which initiate various signaling cascades, partly through phosphorylation^{50,51}. Similarly, many GPCRs mediate tau phosphorylation through neuronal kinases like glycogen synthase kinase 3β, PKA, PKC and ERKs⁵². Abnormal hyperphosphorylation of tau disrupts the neuronal cytoskeleton, impairs axonal transport and impedes tau degradation. These effects collectively contribute to the neurofibrillary pathology and neurodegeneration characteristic of tauopathies. Notably, the cAMP-dependent PKA alone can account for all these detrimental functional consequences 38,53,54.

In our study, we compared the effects of OXR antagonism on the DAG/PKC and cAMP/PKA pathways and found a selective reduction in cAMP levels, accompanied by decreased pPKA, while DAG and pPKC levels remained unchanged. Consistent with these findings, lemborexant-treated male mice exhibited significant reductions in pTau pathology at multiple phosphorylation sites, including Ser202, Thr205 and Ser409, with the latter specifically phosphorylated by PKA³⁸. Tau phosphorylation at individual sites is influenced by both tau conformation and its existing phosphorylation status. Furthermore, PKA's role in tau phosphorylation has been implicated in the early formation of PHFs and the spread of neurofibrillary pathology³⁸. Supporting these results, we also observed reduced levels of aggregated MC1 and PHF1 tau. A limitation of our study is the lack of OXR2-selective inhibition to explore the specific relationship between OXR2 signaling, pTau and tau-mediated neurodegeneration. Future research should include P301S mice lacking OXR2 expression to further clarify this interaction. To address this limitation, we examined the effects of pTau seeding and spreading through both pharmacological inhibition of orexin signaling and genetic deletion of OXR2 expression. These data supported our conclusion that lemborexant likely prevents pTau accumulation primarily via inhibiting OXR2 signaling. Notably, due to the selective vulnerability of orexin-producing neurons in PSP, CBD and AD⁴⁻⁶, further research is required to determine whether tau pathology leads to increased orexin signaling or if a reduction in normal orexin signaling contributes to sleep-wake heterogeneity and neurodegeneration in tauopathies.

The neuroprotective effects were observed exclusively in male P301S/E4 mice treated with lemborexant, in contrast to females. One potential mechanism underlying this differentiation in lemborexant's neuroprotective effects against brain atrophy may involve inhibiting the cAMP/PKA pathway. By blocking this pathway, lemborexant could prevent the accumulation of pPKA-mediated pTau, thereby mitigating tau-mediated neurodegeneration. This reduction in pTau might also contribute to limiting excessive glial reactivity. In addition, it is important to note that cAMP-dependent pPKA activity can influence other tau phosphorylation events through synergistic interactions

with additional kinases⁵⁵. For example, we observed reductions in downstream signaling molecules such as p-p38 MAPK and pERK, which also phosphorylate tau at multiple sites, including Ser202, as detected by AT8. Thus, while the inhibition of pPKA-mediated phosphorylation significantly contributes to the observed reduction in pTau and associated damage, additional contributions cannot be excluded. Given the complexity of modulating neurotransmitter systems and the cAMP/PKA signaling pathway, future studies focusing on individual components in isolation as well as potential sex-specific physiological changes in OXR expression and signaling will be crucial for uncovering detailed underlying mechanisms and expanding our understanding of these pathways in neurodegeneration.

Despite the significant neuroprotection observed in lemborexant-treated male mice, particularly at ZT13, we did not detect corresponding behavioral improvements, except for a relative increase in alternation rate. This may be attributed to the more pronounced reduction of damage in the entorhinal/piriform cortex compared to the hippocampus, as the behavioral tasks used—such as fear conditioning—are primarily hippocampus-dependent measures of memory. Supporting this, many studies have highlighted the roles of AC, cAMP, PKA and MAPK pathways in hippocampus-dependent memory consolidation. For instance, mice lacking calmodulin-stimulated ACs or with disrupted cAMP/PKA signaling perform poorly in hippocampus-dependent tasks such as contextual fear conditioning and passive avoidance ^{56–58}. Future research should explore whether optimizing the timing, duration and dosage of lemborexant treatment can achieve both reduced tau-mediated neurodegeneration and cognitive improvement.

In conclusion, our data support the assessment of lemborexant as a sleep-promoting therapeutic to prevent tau-mediated neurodegeneration. While other GPCRs have been shown to similarly modulate pTau⁵², none so far have demonstrated a protective effect against neurodegeneration. Sleep disturbances are linked to an increased risk of developing AD and are often early indicators of primary tauopathies. In our study, lemborexant-induced sleep occurred in mice that were not sleep deprived. Whether lemborexant treatment could similarly reduce pTau- and tau-mediated neurodegeneration if sleep loss and elevated wakefulness were already present is an important question to address in future studies. Our data suggest that lemborexant may be most effective at reducing pathological tau accumulation when administered before or at earlier stages of sleep disturbances. Given that prolonged wakefulness has been shown to elevate cAMP-mediated PKA phosphorylation and tau production through increased neuronal activity^{10,35,36,57}, it is tempting to speculate that decreasing wake via OXR2 signaling blockade may exert the opposite effect. We currently lack evidence to confirm whether lembor exant can degrade or remove existing tau aggregates, which would help assess its efficacy when treatment begins after sleep loss. Additionally, acute sleep deprivation (up to 5 h) has been shown to reduce cAMP signaling⁵⁸, likely influencing downstream PKA-mediated pTau. However, it remains unclear whether this reduction extends to chronic sleep deprivation or if the acute response is sustained over time. Our study highlights the importance of early therapeutic intervention in mitigating sleep-wake disturbances, as well as in slowing or preventing neurodegeneration in tauopathies.

Online content

Any methods, additional references, Nature Portfolio reporting summaries, source data, extended data, supplementary information, acknowledgements, peer review information; details of author contributions and competing interests; and statements of data and code availability are available at https://doi.org/10.1038/s41593-025-01966-7.

References

 Bubu, O. M. et al. Obstructive sleep apnea, cognition and Alzheimer's disease: a systematic review integrating three decades of multidisciplinary research. Sleep. Med. Rev. 50, 101250 (2020).

- Shi, L. et al. Sleep disturbances increase the risk of dementia: a systematic review and meta-analysis. Sleep. Med. Rev. 40, 4–16 (2018).
- Lew, C. H., Petersen, C., Neylan, T. C. & Grinberg, L. T. Tau-driven degeneration of sleep- and wake-regulating neurons in Alzheimer's disease. Sleep. Med. Rev. 60, 101541 (2021).
- 4. Eser, R. A. et al. Selective vulnerability of brainstem nuclei in distinct tauopathies: a postmortem study. *J. Neuropathol. Exp. Neurol.* **77**, 149–161 (2018).
- Oh, J. et al. Profound degeneration of wake-promoting neurons in Alzheimer's disease. Alzheimers Dement. 15, 1253–1263 (2019).
- Parhizkar, S. & Holtzman, D. M. The night's watch: exploring how sleep protects against neurodegeneration. *Neuron* 113, 817–837 (2025).
- Malpetti, M., La Joie, R. & Rabinovici, G. D. Tau beats amyloid in predicting brain atrophy in Alzheimer disease: implications for prognosis and clinical trials. J. Nucl. Med. 63, 830–832 (2022).
- Lucey, B. P. et al. Reduced non-rapid eye movement sleep is associated with tau pathology in early Alzheimer's disease. Sci. Transl. Med. 11, eaau6550 (2019).
- Holth, J. K., Mahan, T. E., Robinson, G. O., Rocha, A. & Holtzman, D. M. Altered sleep and EEG power in the P301S Tau transgenic mouse model. *Ann. Clin. Transl. Neurol.* 4, 180–190 (2017).
- 10. Holth, J. K. et al. The sleep–wake cycle regulates brain interstitial fluid tau in mice and CSF tau in humans. *Science* **363**, 880–884 (2019)
- Zhu, Y. et al. Chronic sleep disruption advances the temporal progression of tauopathy in P301S mutant mice. J. Neurosci. 38, 10255–10270 (2018).
- Verster, J. C. et al. Residual effects of middle-of-the-night administration of zaleplon and zolpidem on driving ability, memory functions, and psychomotor performance. J. Clin. Psychopharmacol. 22, 576–583 (2002).
- Morgan, P. T., Kehne, J. H., Sprenger, K. J. & Malison, R. T. Retrograde effects of triazolam and zolpidem on sleep-dependent motor learning in humans. J. Sleep. Res. 19, 157–164 (2010).
- Robbins, R. et al. Sleep medication use and incident dementia in a nationally representative sample of older adults in the US. Sleep. Med. 79, 183–189 (2021).
- Donnelly, K., Bracchi, R., Hewitt, J., Routledge, P. A. & Carter, B. Benzodiazepines, Z-drugs and the risk of hip fracture: a systematic review and meta-analysis. *PLoS ONE* 12, e0174730 (2017).
- Sakurai, T. et al. Orexins and orexin receptors: a family of hypothalamic neuropeptides and G protein-coupled receptors that regulate feeding behavior. Cell 92, 573–585 (1998).
- de Lecea, L. et al. The hypocretins: hypothalamus-specific peptides with neuroexcitatory activity. *Proc. Natl Acad. Sci. USA* 95, 322–327 (1998).
- Herring, W. J. et al. Polysomnographic assessment of suvorexant in patients with probable Alzheimer's disease dementia and insomnia: a randomized trial. Alzheimers Dement. 16, 541–551 (2020).
- Moline, M. et al. Safety and efficacy of lemborexant in patients with irregular sleep-wake rhythm disorder and Alzheimer's disease dementia: results from a phase 2 randomized clinical trial. J. Prev. Alzheimers Dis. 8, 7–18 (2021).
- 20. Lucey, B. P. et al. Suvorexant acutely decreases tau phosphorylation and A β in the human CNS. *Ann. Neurol.* **94**, 27–40 (2023).
- Beuckmann, C. T., Ueno, T., Nakagawa, M., Suzuki, M. & Akasofu, S. Preclinical in vivo characterization of lemborexant (E2006), a novel dual orexin receptor antagonist for sleep/wake regulation. Sleep 42, zsz076 (2019).

- Murphy, P. et al. Lemborexant, a dual orexin receptor antagonist (DORA) for the treatment of insomnia disorder: results from a Bayesian, adaptive, randomized, double-blind, placebo-controlled study. J. Clin. Sleep. Med. 13, 1289–1299 (2017).
- Yardley, J. et al. Long-term effectiveness and safety of lemborexant in adults with insomnia disorder: results from a phase 3 randomized clinical trial. Sleep. Med. 80, 333–342 (2021).
- 24. Kang, J. E. et al. Amyloid-β dynamics are regulated by orexin and the sleep-wake cycle. *Science* **326**, 1005–1007 (2009).
- Roh, J. H. et al. Potential role of orexin and sleep modulation in the pathogenesis of Alzheimer's disease. J. Exp. Med. 211, 2487–2496 (2014).
- 26. Josephs, K. A. et al. β -Amyloid burden is not associated with rates of brain atrophy. *Ann. Neurol.* **63**, 204–212 (2008).
- Shi, Y. et al. ApoE4 markedly exacerbates tau-mediated neurodegeneration in a mouse model of tauopathy. *Nature* 549, 523–527 (2017).
- Yoshiyama, Y. et al. Synapse loss and microglial activation precede tangles in a P301S tauopathy mouse model. *Neuron* 53, 337–351 (2007).
- 29. Shi, Y. et al. Microglia drive APOE-dependent neurodegeneration in a tauopathy mouse model. *J. Exp. Med.* **216**, 2546–2561 (2019).
- Mancuso, R. et al. CSF1R inhibitor JNJ-40346527 attenuates microglial proliferation and neurodegeneration in P301S mice. *Brain* 142, 3243–3264 (2019).
- Keenan, R. J. et al. Differential sleep/wake response and sex differences following acute suvorexant, MK-1064 and zolpidem administration in the rTg4510 mouse model of tauopathy. Br. J. Pharmacol. 179, 3403–3417 (2022).
- 32. Chen, X. et al. Microglia-mediated T cell infiltration drives neurodegeneration in tauopathy. *Nature* **615**, 668–677 (2023).
- Krasemann, S. et al. The TREM2-APOE pathway drives the transcriptional phenotype of dysfunctional microglia in neurodegenerative diseases. *Immunity* 47, 566-581 (2017).
- 34. Keren-Shaul, H. et al. A unique microglia type associated with restricting development of Alzheimer's disease. *Cell* **169**, 1276–1290 (2017).
- 35. Yamada, K. et al. Neuronal activity regulates extracellular tau in vivo. *J. Exp. Med.* **211**, 387–393 (2014).
- 36. Wu, J. W. et al. Neuronal activity enhances tau propagation and tau pathology in vivo. *Nat. Neurosci.* **19**, 1085–1092 (2016).
- 37. Ahmed, Z. et al. A novel in vivo model of tau propagation with rapid and progressive neurofibrillary tangle pathology: the pattern of spread is determined by connectivity, not proximity. *Acta Neuropathol.* **127**, 667–683 (2014).
- Jicha, G. A. et al. cAMP-dependent protein kinase phosphorylations on tau in Alzheimer's disease. *J. Neurosci.* 19, 7486–7494 (1999).
- Beuckmann, C. T. et al. In vitro and in silico characterization of lemborexant (E2006), a novel dual orexin receptor antagonist. J. Pharmacol. Exp. Ther. 362, 287–295 (2017).
- Guo, J. L. et al. Unique pathological tau conformers from Alzheimer's brains transmit tau pathology in nontransgenic mice.
 J. Exp. Med. 213, 2635–2654 (2016).
- Walsh, C. M. et al. Sleepless night and day, the plight of progressive supranuclear palsy. Sleep 40, zsx154 (2017).
- 42. McCurry, S. M. et al. Characteristics of sleep disturbance in community-dwelling Alzheimer's disease patients. *J. Geriatr. Psychiatry Neurol.* **12**, 53–59 (1999).
- 43. Keenan, R. J. et al. Orexin 2 receptor antagonism sex-dependently improves sleep/wakefulness and cognitive performance in tau transgenic mice. *Br. J. Pharmacol.* **181**, 87–106 (2024).
- Gratuze, M. et al. TREM2-independent microgliosis promotes tau-mediated neurodegeneration in the presence of ApoE4. Neuron 111, 202–219 (2023).

- Zhang, Y. et al. An RNA-sequencing transcriptome and splicing database of glia, neurons, and vascular cells of the cerebral cortex. J. Neurosci. 34, 11929–11947 (2014).
- 46. Liu, Y. U. et al. Neuronal network activity controls microglial process surveillance in awake mice via norepinephrine signaling. *Nat. Neurosci.* **22**, 1771–1781 (2019).
- 47. Stowell, R. D. et al. Noradrenergic signaling in the wakeful state inhibits microglial surveillance and synaptic plasticity in the mouse visual cortex. *Nat. Neurosci.* **22**, 1782–1792 (2019).
- Small, K. M., Brown, K. M., Forbes, S. L. & Liggett, S. B. Polymorphic deletion of three intracellular acidic residues of the α2B-adrenergic receptor decreases G protein-coupled receptor kinase-mediated phosphorylation and desensitization. *J. Biol. Chem.* 276, 4917–4922 (2001).
- Ijiro, T. et al. Effect of rovatirelin, a novel thyrotropin-releasing hormone analog, on the central noradrenergic system. Eur. J. Pharmacol. 761, 413–422 (2015).
- 50. Leonard, C. S. & Kukkonen, J. P. Orexin/hypocretin receptor signalling: a functional perspective. *Br. J. Pharmacol.* **171**, 294–313 (2014).
- Kukkonen, J. P. & Leonard, C. S. Orexin/hypocretin receptor signalling cascades. Br. J. Pharmacol. 171, 314–331 (2014).
- Chidambaram, H. & Chinnathambi, S. G-Protein coupled receptors and tau-different roles in Alzheimer's disease. Neuroscience 438, 198–214 (2020).
- Scott, C. W. et al. Phosphorylation of recombinant tau by cAMP-dependent protein kinase. Identification of phosphorylation sites and effect on microtubule assembly. J. Biol. Chem. 268, 1166–1173 (1993).

- Illenberger, S. et al. The endogenous and cell cycle-dependent phosphorylation of tau protein in living cells: implications for Alzheimer's disease. Mol. Biol. Cell 9, 1495–1512 (1998).
- 55. Liu, F. et al. PKA modulates GSK-3β- and cdk5-catalyzed phosphorylation of tau in site- and kinase-specific manners. *FEBS Lett.* **580**, 6269–6274 (2006).
- Luo, J., Phan, T. X., Yang, Y., Garelick, M. G. & Storm, D. R. Increases in cAMP, MAPK activity, and CREB phosphorylation during REM sleep: implications for REM sleep and memory consolidation. *J. Neurosci.* 33, 6460–6468 (2013).
- Abel, T. et al. Genetic demonstration of a role for PKA in the late phase of LTP and in hippocampus-based long-term memory. Cell 88, 615–626 (1997).
- 58. Vecsey, C. G. et al. Sleep deprivation impairs cAMP signalling in the hippocampus. *Nature* **461**, 1122–1125 (2009).

Publisher's note Springer Nature remains neutral with regard to jurisdictional claims in published maps and institutional affiliations.

Springer Nature or its licensor (e.g. a society or other partner) holds exclusive rights to this article under a publishing agreement with the author(s) or other rightsholder(s); author self-archiving of the accepted manuscript version of this article is solely governed by the terms of such publishing agreement and applicable law.

© The Author(s), under exclusive licence to Springer Nature America, Inc. 2025

Methods

Animals

All animal procedures and protocols were approved by the Institutional Animal Care and Use Committee at Washington University School of Medicine (IACUC-24-0098). PS19 tau transgenic mice harboring 1N4R tau (Jackson Laboratory, 008169) and overexpressing human P301S tau mutation were used²⁸. These mice have been backcrossed to C57BL/6 for more than ten generations. Human APOE4 knock-in mice were generated by replacing the mouse genomic sequence from the translation initiation codon in exon 2 to the termination codon in exon 4 with its human counterparts flanked by loxP sites⁵⁹. P301S tau transgenic mice on a C57BL/6 background were crossed with human ApoE KI mice to generate P301S/E4 mice and bred for several generations to produce experimental mice. OXR2 knockout mice 60 on C57BI/6I background were used. Both male and female P301S/E4 animals and only male OXR2 wild-type and knockout mice were used and killed at 9.5 months of age. All mice were housed in specific pathogen-free conditions, maintained under a consistent 12-h light/12-h dark cycle, with ambient room temperatures ranging from 20 °C to 26 °C and humidity levels between 30% and 70%. Food and water were available ad libitum.

Randomization and blinding

For all animal experiments, mice were randomly assigned to experimental groups that were matched by sex, littermate and age using the RAND function in Microsoft Excel following genotyping. All identifying numbers for the mice were pseudonymized, and the investigator remained blinded to these identifiers, ensuring that all experiments and analyses were conducted in a blinded manner. Investigators were unblinded for statistical analyses. No statistical methods were used to predetermine sample sizes. However, our sample sizes were based on experience from our previous findings^{27,32}.

Lemborexant, zolpidem or vehicle treatment

Lemborexant was obtained from Eisai. Zolpidem was purchased from Sigma-Aldrich. Mice were gavaged daily with a single 30 mg kg⁻¹ dose of lemborexant, zolpidem or 0.5% methylcellulose vehicle at ZT3 or ZT13, starting at 7.5 months of age until killing at 9.5 months of age.

Measurement and analysis of sleep-wake states

Sleep-wake behavior in mice was monitored using two independent methods. EEG and the PiezoSleep mouse behavioral tracking system (Signal Solutions). Mice were simultaneously gavaged daily with lemborexant, zolpidem or vehicle throughout the experiments until killed. For EEG experiments, 8.5-month-old mice were anesthetized with isoflurane (0.5-3%). Before incision, the depth of anesthesia was assessed by toe pinch. Mice were then surgically implanted with screw electrodes in the skull for EEG and stainless wire electrodes in the nuchal muscle for electromyography (EMG). After a midline vertical incision to expose the skull, forceps and 3% hydrogen peroxide were used to remove any connective tissue and dry the skull for electrode placement. Burr holes for the frontal reference electrodes were made (anterior, ± 0.5 mm and lateral, ± 0.5 mm; bregma) using a micro drill with a 0.9 mm tip, and screws were secured in the skull. Two bilateral active recording electrodes were placed over the parietal cortex (posterior, -2.5 mm and lateral, ±1.5; bregma), and a ground screw was secured over the cerebellum (posterior, -6.2 mm and lateral, ±0.5; bregma), using the same technique as the reference electrode. The exposed skull, screws and all wires were covered in a layer of dental cement (SNAP, Parkell), with the pin header secured to the head for subsequent recording. The skin was sutured around the exposed dental cement/ pin header, and tissue glue (Vetbond; 3 months) was used to close the remainder of the incision. After the procedure, mice were placed in a warmed chamber to fully recover from anesthesia and individually housed in monitoring cages with fresh bedding, water and food ad libitum. Three days after surgery, mice were tethered and habituated

in the recording cage for 2 weeks, followed by undisturbed EEG/EMG recording for two consecutive days. Bilateral cortical EEG signals were acquired by a P511K A.C. Preamplifier (Grass-Telefactor Instruments), digitized with a BIOPAC MP150, recorded digitally using the BIOPAC's AcqKnowledge 5.0 software with a sampling rate of 250 Hz and converted into (.edf) format for analysis. EEG was processed in MATLAB (MathWorks) through a band-pass filter of 1–30 Hz to remove direct current offset and high-frequency noise. EEG/EMG recordings were manually scored in 10-s epochs for wake, NREM and REM sleep to create a calibration file containing mixture z-scoring variables specific to the recording subject. The calibration file was imported into AccuSleep, a machine learning-based, automated sleep scoring program in MATLAB, to complete the remainder of the scoring⁶¹.

We additionally used the PiezoSleep mouse behavioral tracking system (Signal Solutions), as described previously 62 . Mice were individually housed with the piezo pad underneath fresh bedding, with fresh water and food available ad libitum and recorded without disturbance over a period of 6 days. Data were acquired using SleepStats software (Signal Solutions, v2.18).

Tissue collection

All mice were perfused between ZT3 and ZT7 to avoid circadian influence on transcriptional fluctuation of gene expression. Before transcardiac perfusion, mice were anesthetized with pentobarbital (50 mg kg $^{-1}$, intraperitoneal). Blood was collected from the heart before transcardiac perfusion, which was centrifuged at 5,000g for 5 min at 4 °C to obtain plasma. Mice were transcardially perfused with ice-cold phosphate-buffered saline containing 0.3% heparin. One hemibrain was dissected, snap frozen and stored at -80 °C for biochemical analyses. The other hemibrain was immersion-fixed for 24 h in 4% paraformaldehyde, followed by cryoprotection in 30% sucrose for 48 h, and frozen at -80 °C until tissue samples were sectioned for immunohistochemical analyses.

NFL concentration

Plasma NFL concentration was measured with the NF-Light Simoa Assay Advantage kit using Quanterix SIMOA HD-X. The measurement was performed following the manufacturer's instructions.

Volumetric analysis

Volumetric analysis of the hippocampus, entorhinal/piriform cortex and ventricle was performed via stereological methods by assessing sections spaced by 180 μ m starting from bregma –1.3 mm to bregma –3.1 mm (16–18 sections per mouse, depending on the severity of brain atrophy). The 30 μ m microtome-cut sections mounted on slides were briefly immersed in distilled water before incubating in prewarmed 0.1% cresyl violet at 37 °C for 6 min. Following this, tissues were rinsed in distilled water and transferred to 70%, 95% and 100% ethanol sequentially for 2 min each. Slides were then cleared in xylene before finally coverslipping with cytoseal60 mounting medium (Thermo Fisher Scientific). Slides were scanned using Hamamatsu's Nanozoomer microscope at ×20 magnification. Hippocampus, entorhinal/piriform cortex and ventricles were traced using NDP.view 2. The formula for the volumetric calculation was volume = (sum of area) × 0.3 mm.

Neuronal layer thickness measurement

Dentate granular and entorhinal pyramidal cell layers were measured across three sections by drawing a scale line across the cell layer using NDP.view 2 and calculating the average value for each mouse.

Immunohistochemistry

Free-floating sections (n=3 tissue sections as technical replicates per mouse) were briefly washed with tris(hydroxymethyl)aminomethane (TRIS)-buffered saline with 1% Triton X-100 (TBS-Tx) before quenching endogenous peroxidase with 0.3% hydrogen peroxide for 20 min at

room temperature. After a brief wash, sections were blocked using 5% goat serum for 30 min at room temperature, followed by primary antibody incubation in biotinylated AT8 (Phospho-Tau Ser202, Thr205; Thermo Fisher Scientific, MN1020B; 1:500), PG5 or MC1 (1:500; kindly gifted by P. Davies) overnight at 4 °C. The following day, PG5- and MC1-stained sections were briefly washed and incubated in horseradish peroxidase (HRP)-conjugated secondary antibody for 1 h at room temperature. AT8-, PG5- and MC1-stained tissue were then developed with 3,3'-diaminobenzidine (Sigma) for 10 min, 14 min and 20 min, respectively. Tissue sections were mounted on slides and dehydrated using a series of increasingly concentrated ethanol before finally immersing them in xylene and coverslipping using Cytoseal mounting medium. Slides were scanned using Hamamatsu's Nanozoomer microscope at ×20 magnification.

Immunofluorescence stainings

Free-floating sections (n = 3 tissue sections as technical replicates per mouse) were washed briefly with PBS and blocked in 5% donkey serum for 1 h at room temperature. Primary antibodies were diluted in blocking buffer and incubated at 4 °C overnight with slow agitation unless stated otherwise. Primary antibodies were used as follows: Iba1 (Fujifilm, 019-19741; 1:500 or Novus Biologicals, NB100-1028), Cd68 (Bio-Rad, FA-11; 1:1,000), Tmem119 (Cell Signaling Technology, E3E1O; 1:500), Clec7a (1:50 at room temperature; mabg-mdect; InvivoGen), Gfap (2E1.E9 Alexa Fluor 488-conjugated, 1:2,000; BioLegend), ApoE (Cell Signaling Technology, D7I9N; 1:300), Psd95 (Thermo Fisher Scientific, 51-6900; 1:200) and Vglut1 (Merck Millipore, AB5905; 1:200). The following day, sections were washed and incubated with secondary antibody diluted in blocking buffer (donkey anti-rabbit IgG (H+L)-AlexaFluor647, 1:1,000 (Thermo Fisher Scientific); donkey anti-rabbit IgG (H+L)-AlexaFluor594, 1:1,000 (Thermo Fisher Scientific); donkey anti-goat IgG (H+L)-AlexaFluor594, 1:1,000 (Thermo Fisher Scientific); donkey anti-goat IgG (H + L)-AlexaFluor647,1:1,000 (Thermo Fisher Scientific); donkey anti-rat IgG(H+L)-AlexaFluor488, 1:1,000 (Thermo Fisher Scientific); goat anti-guinea pig IgG(H + L)-AlexaFluor488, 1:500 (Thermo Fisher Scientific); goat anti-rabbit IgG (H + L)-AlexaFluor594, 1:500 (Thermo Fisher Scientific)), followed by a 4',6-diamidin-2-phenylindol (5 µg ml⁻¹) where appropriate before mounting sections onto slides (Prolong Gold Antifade reagent; Thermo Fisher Scientific).

Confocal imaging and analyses

Images were acquired using a Leica Stellaris 5 confocal microscope and Leica Application Suite X software (4.2.1.23810). Laser and detector settings were maintained constant for the acquisition of each immunostaining. For all analyses, at least two images were taken per brain region and slide using ×20 (Apo CS ×10/0.40 dry), ×40 (Apo CS ×40.0/1.25) and ×63 (Apo CS ×63.0/1.4 oil) differential interference contrast objectives, respectively, at 1,024 × 1,024 pixel resolution, with a 15 µm z-step thickness. For imaging synapses, Leica Stellaris 8 Lightning was used to produce adaptive deconvolution-based super-resolved confocal images using a ×63 oil objective. Image analysis was performed using FIJI (ImageJ2, 2.14.0/1.54f). For the feasibility of the quantification, all layers from a single image stack were projected on a single slice (Stack\Z projection). Next, glia were segmented using automatic thresholding methods in FIJI and presented as the percentage area covered by the selected stain in the hippocampus or the entorhinal/ piriform cortex.

Protein extraction

Frozen mouse piriform/entorhinal tissue was weighed and homogenized in a bullet blender homogenizer (Next Advance) using beaded tubes with 200 µl reassembly (RAB) buffer pH 7.0 (100 mM 2-(*N*-morpholino)ethanesulfonic acid, 1 mM ethyleneglycol bis(2-aminoethyl ether)-*N*,*N*,*N*, *N*, tetraacetic acid, 0.5 mM MgSO₄,

750 mM NaCl, 20 mM NaF and 1 mM Na₃VO₄) supplemented with 1× protease inhibitor (cOmplete: Roche) and 1× phosphatase inhibitor (PhosSTOP; Roche). This homogenate was centrifuged for 5 min at 4 °C at 5,000g to pellet RAB insoluble material, and the supernatant was ultracentrifuged for 20 min at 50,000g with an MLA-130 rotor in an Optima MAX-XP ultracentrifuge (Beckman Coulter) to obtain the RAB extracts. From the remaining cellular pellet, proteins were extracted with RIPA buffer pH 8.0 (150 mM NaCl, 50 mM TRIS, 0.5% deoxycholic acid, 1% Triton X-100, 0.1% sodium deoxycholate, 5 mM EDTA, 20 mM NaF and 1 mM Na₃VO₄) supplemented with protease and phosphatase inhibitors. After a 5-min clearing for RIPA-insoluble material at 5,000g at 4 °C, the supernatant was again ultracentrifuged for 30 min at 50,000g to obtain the RIPA-soluble protein fraction. The RIPA-insoluble pellet was dissolved with ice-cold 70% formic acid and sonicated for 1 min at 30% amplitude in short pulses at room temperature using sonicator (Thermo Fisher Scientific, model FB120), followed by a final ultracentrifugation for 20 min at 50,000g at 4 °C. Protein concentrations were measured in technical duplicates for RIPA fractions using a bicinchoninic acid (BCA) assay (Pierce). All samples were aliquoted and frozen at -80 °C until use.

SDS-PAGE and immunoblotting

In total, 10 µg of total protein mixed with 4× Laemmli sample buffer was loaded and separated by 4-20% Mini-PROTEAN TGX gels in TRIS/ glycine/SDS running buffer (Bio-Rad). Gels were then transferred onto a PVDF membrane using the Trans-Blot Turbo Transfer System (Bio-Rad). After protein transfer, the membrane was blocked with 5% bovine serum albumin in TBS with 0.1% Triton X-100 (TBST) for 30 min at room temperature. Primary antibodies were used at 1:1,000 at 4 °C overnight as follows unless otherwise stated: PKC (Cell Signaling Technology, 46809S), phospho-PKC (Cell Signaling Technology, 38938S), PKA (Cell Signaling Technology, 4782S), phospho-PKA (Cell Signaling Technology, 4781S), ERK1/ERK2 (Cell Signaling Technology, 4695S), phospho-Erk (Cell Signaling Technology, 4370S), p38 (Cell Signaling Technology, 8690S), phospho-p38 (Cell Signaling Technology, 4511S), AT8 (Thermo Fisher Scientific, MN1020B; 1:500), PHF1 (kindly gifted by P. Davies) and GAPDH (Proteintech, HRP-60004; 1:2,000). The next day, membranes were washed and incubated in HRP-conjugated secondary antibodies (goat anti-rabbit HRP, 1:5,000 (Thermo Fisher Scientific); goat anti-mouse HRP, 1:5,000 (Thermo Fisher Scientific)) for 60 min at room temperature, followed by a series of washes. Membranes were developed using ECL Western Blotting Substrate (Thermo Fisher Scientific) and imaged by ChemiDoc Imaging Systems (Bio-Rad).

DAG and cAMP ELISAs

Entorhinal/piriform cortex brain lysates were used to quantify DAG (Abbexa, abx258320) and cAMP (Arbor Assays, K019-H) using the manufacturer's protocol. RIPA samples were adjusted using the manufacturer's protocol and measured in duplicates.

General design of behavioral tests

Mice were transferred to the Washington University Animal Behavior Core 1 week before behavioral testing. Following habituation, mice were assessed for spontaneous alternation in the Y-maze and fear conditioning. All behavioral testing was conducted after ZT6 to avoid disturbing lemborexant-induced sleep shortly after gavage.

Spontaneous alternation Y-maze

Individual mice were placed in one arm of a Y-maze featuring three arms, each measuring 10.5 cm in width, 40 cm in length and 20.5 cm in depth, with each arm oriented at a 120° angle to the next. Mice were given 8 min to explore the maze, and an entry into an arm was recorded only when the hindlimbs had fully entered. An alternation was defined as three consecutive choices of three different arms without revisiting

any previously explored arm. The dependent variables included the number of alternations, arm entries and the percentage of alternations, calculated by dividing the total number of alternations by the total number of entries minus 2, and then multiplying by 100.

Conditioned fear

Fear conditioning was assessed to train and test mice in two distinct clear-plastic conditioning chambers ($26 \times 18 \times 18$ cm high; Med-Associates), each identifiable by unique olfactory, visual, and tactile cues (chamber 1-metal grid floor, metal walls and mint scent; chamber 2—solid acrylic floor, black acrylic walls and coconut scent). On the first day, each mouse was placed in chamber 1 for 5 min, during which freezing behavior was measured over a 2-min baseline period. Freezing, defined as no movement except for respiration, was analyzed using FreezeFrame image analysis software (Actimetrics), which allowed for real-time visualization of behavior while setting a 'freezing threshold' during 0.75-s intervals. Following the baseline, a conditioned stimulus (CS) consisting of an 80 dB tone (white noise) was presented for 20 s, followed by an unconditioned stimulus of a 1-s, 1.0 mA continuous foot shock. This T/S pairing was repeated every minute for the next 2 min, with freezing behavior recorded after each of the three pairings. Twenty-four hours post-training, each mouse was returned to chamber 1 to assess fear conditioning to the contextual cues, measuring freezing behavior over an 8-min period without the tone or shock. Forty-eight hours after the contextual test, the mice underwent evaluation for the auditory cue component of the conditioned fear procedure, which involved placing them in chamber 2 with distinctly different cues. Freezing was quantified during a 2-min baseline period in the altered context, followed by an 8-min period during which the auditory cue (CS) was presented.

AD-tau extraction

AD-tau was isolated from a human AD brain, Braak stage VI. In brief, frontal cortical gray matter from human AD brains was homogenized using a Dounce homogenizer in nine volumes (vol/wt) of high-salt buffer containing 10 mM TRIS-HCl (pH 7.4), 0.8 M NaCl, 1 mM EDTA, 2 mM dithiothreitol, protease inhibitor cocktail, phosphatase inhibitors, phenylmethanesulfonyl fluoride, 0.1% sarkosyl and 10% sucrose. The homogenate was centrifuged at 10,000g for 10 min at 4 °C, and the resulting pellet was re-extracted twice under the same conditions. The supernatants were filtered, pooled and supplemented with sarkosyl to a final concentration of 1%. Following a 1-h rotation at room temperature, the samples were centrifuged at 300,000g for 60 min at 4 °C. The resulting 1% sarkosyl-insoluble pellets, enriched in pathological tau, were washed once with PBS and resuspended in PBS (~100 μl g⁻¹ gray matter) by passing the suspension through 27-gauge needles. The sarkosyl-insoluble fraction was further purified by brief sonication (20 pulses at ~0.5 s per pulse) and centrifugation at 100,000g for 30 min at 4 °C. The resulting pellets were resuspended in PBS at one-fifth to half of the original volume, subjected to 20-60 short sonication pulses (~0.5 s per pulse) and centrifuged at 10,000g for 30 min at 4 °C to remove large debris. Stock preparations were aliquoted and frozen at -80 °C until further use. Before injection, each vial was thawed on ice and sonicated in a water bath sonicator (QSonica, Q700) for 30 s at 60% amplitude at 4 °C.

Intrahippocampal injections

Seven-month-old OXR2^{WT} and OXR2^{KO} mice were anesthetized using isoflurane and immobilized on a stereotaxic frame (Kopf Instruments). In total, 8 µg of AD-tau (4 µg at each injection site) in the dentate gyrus (bregma, -2.5 mm; lateral, -2.0 mm; depth, -2.2 mm) and overlying cortex (bregma, -2.5 mm; lateral, -2.0 mm; depth, -1.0 mm) was bilaterally injected using a Hamilton syringe (Hamilton; syringe, 80265–1702RNR; needle, 7803–07). The incision was cleaned with povidone-iodine antiseptic solution and sutured. Mice were allowed to recover on a

37 °C heating pad and returned to clean cages upon recovery. Mice were monitored for 72 h following surgery.

RNA extraction

Frozen cortical tissue was weighed and homogenized in RNAase-free beaded tubes (REDE, Next Advance) in chloroform with TRIzol. Samples were centrifuged for 15 min at 12,000g at 4 °C, and the aqueous upper supernatant was transferred for RNA isolation with the RNeasy Mini Kit (Qiagen) following the manufacturer's instructions. RNA quality was controlled using the Bioanalyzer before Next Generation Sequencing by Clontech SMARTer.

Real-time quantitative PCR

RNA was reverse transcribed to cDNA using the high-capacity RNA-to-cDNA kit (Applied Biosystems, 4387406) following the manufacturer's instructions. Quantitative PCR was performed with Taqman primers (Adcyl ID, Mm01187829_m1; Prkacb ID, Mm01312555_m1; Prkaca ID, Mm00660092_m1; Hcrt1 ID, Mm01185776_m1; Hcrt2 ID, Mm01179312_m1; Dag1 ID, Mm00802400_m1; Camp ID, Mm00438285_m1; Prkca ID, Mm00440858_m1; Prkcb ID, Mm00435749_m1; Thermo Fisher Scientific) and Taqman universal PCR master mix (Applied Biosystems, 4304437) using the QuantStudio 12K Flex Real-Time PCR System (Applied Biosystems). Data were normalized to the geometric mean values of β -actin (ID, Mm01205647_g1) and Gapdh (ID, Mm99999915_g1).

RNA-seq and analyses

Total RNA integrity was determined using an Agilent Bioanalyzer or 4200 TapeStation. Library preparation was performed with 10 ng of total RNA with a Bioanalyzer RIN score greater than 8.0. ds-cDNA was prepared using the SMARTer Ultra Low RNA kit for Illumina Sequencing (Takara-Clontech) per the manufacturer's protocol. cDNA was fragmented using a Covaris E220 sonicator using peak incident power 18, duty factor 20% and cycles per burst 50 for 120 s. cDNA was blunt-ended, had an A base added to the 3' ends and then had Illumina sequencing adapters ligated to the ends. Ligated fragments were then amplified for 12-15 cycles using primers incorporating unique dual index tags. Fragments were sequenced on an Illumina NovaSeq 6000 using paired-end reads extending 150 bases. RNA-seg reads were then aligned and quantified to the Ensembl release 101 primary assembly with an Illumina DRAGEN Bio-IT on-premise server running software (3.9.3-8). All gene counts were then imported into the R package (4.1.1). EdgeR (3.36.0) and trimmed mean of M-values (TMM) normalization size factors were calculated to adjust for samples for differences in library size. Ribosomal genes and genes not expressed in the smallest group size minus one sample greater than one count-per-million were excluded from further analysis. The TMM size factors and the matrix of counts were then imported into the R/Bioconductor package Limma (3.50.0). Weighted likelihoods based on the observed mean-variance relationship of every gene and sample were then calculated for all samples with the voomWithQualityWeights function and were fitted using a Limma generalized linear model with additional unknown latent effects as determined by surrogate variable analysis (sva package v.3.42.0). The performance of all genes was assessed with plots of the residual s.d. of every gene to their average log-count with a robustly fitted trend line of the residuals. Differential expression analysis was then performed to analyze for differences between conditions, and the results were filtered for only those genes with Benjamini-Hochberg false-discovery rate adjusted P values less than or equal to 0.05.

Statistical analyses

GraphPad Prism 10.0 was used for all statistical analyses. Data are presented as mean \pm s.e.m. of biological replicates. Outliers were identified using ROUT analysis with a Q value of 1%. Samples were excluded from the sleep experiments if the data demonstrated substantial noise

after filtration, compromising their reliability. Additionally, mice that were too sick to undergo behavioral assessments were excluded to prioritize animal welfare and preserve the accuracy and consistency of the experimental results. For immunohistochemistry experiments, samples were excluded if the tissue integrity was compromised in one or more of the replicates. For biochemistry experiments, samples were excluded if the sample quality was compromised by, for example, impurity, low protein yield or pipetting inconsistencies across technical replicates. Normality was assessed through the Shapiro-Wilk method, D'Agostino and Pearson normality test and the KS normality test. Based on these assessments, statistical significance between groups was determined using a two-tailed t test, one-way analysis of variance (ANOVA) or Kruskal-Wallis test, followed by Dunnett's or Dunn's post hoc test, respectively. For multifactorial datasets, a two-way ANOVA followed by Dunnett's post hoc test was applied for group-wise comparisons unless stated otherwise. Further details on statistics are available as Supplementary Information. Pvalue less than 0.05 was considered significant -*P < 0.05, **P < 0.01 and ***P < 0.001.

Reporting summary

Further information on research design is available in the Nature Portfolio Reporting Summary linked to this article.

Data availability

Numerical source data files are available as supplementary data files. RNA-seq data are publicly available from the Gene Expression Omnibus under accession code GSE283736. Source data are provided with this paper.

References

- Huynh, T.-P. V. et al. Lack of hepatic apoE does not influence early Aβ deposition: observations from a new APOE knock-in model. Mol. Neurodegener. 14, 37 (2019).
- Willie, J. T. et al. Distinct narcolepsy syndromes in orexin receptor-2 and orexin null mice. *Neuron* 38, 715–730 (2003).
- Barger, Z., Frye, C. G., Liu, D., Dan, Y. & Bouchard, K. E. Robust, automated sleep scoring by a compact neural network with distributional shift correction. PLoS ONE 14, e0224642 (2019).
- Yaghouby, F., Donohue, K. D., O'Hara, B. F. & Sunderam, S. Noninvasive dissection of mouse sleep using a piezoelectric motion sensor. J. Neurosci. Methods 259, 90–100 (2016).

Acknowledgements

We thank Eisai for providing lemborexant. We would like to thank the Genome Technology Access Center in the Department of Genetics at Washington University School of Medicine for help with genomic analysis. This study was supported by the National Institutes of Health (grants P01NS074969, RF1NS090934 and RF1AG061776 to D.M.H.), the Freedom Together Foundation (to D.M.H.), the Alzheimer's Association (AARF-21-850865 to S.P.) and the COBRAS Feldman Fellowship (to S.P.).

Author contributions

S.P. and D.M.H. designed the study. S.P. and X.B. orally gavaged the mice and collected and analyzed the Piezosleep data. S.P., X.B., C.L., G.G. and J.R.S. perfused and collected samples. N.R., W.C., S.P., E.C.L. and M.W. collected and analyzed all EEG/EMG data. Y.C. and S.S. performed the AD-tau extract preparation and intrahippocampal injections. E.T. performed the RNA-sequencing analysis. S.P., X.B., G.G., M.K. and E.F. performed and analyzed the immunohistochemistry, imaging, RNA and protein extraction, qPCR, immunoblotting and ELISA experiments. M.M. and X.B. performed and analyzed the NFL SIMOA data. S.P., X.B., G.G. and M.E.B. maintained the mouse colony. C.M.Y. collected and analyzed all behavioral experiments. S.P. wrote the draft. D.M.H. reviewed and edited the paper. All authors discussed the results and commented on the paper.

Competing interests

D.M.H. is an inventor on a patent licensed by Washington University to C2N Diagnostics on the therapeutic use of anti-tau antibodies; cofounded and is on the scientific advisory board of C2N Diagnostics; is on the scientific advisory board of Denali, Genentech, Cajal Neuroscience and Switch Therapeutics and consults for Pfizer and Roche. The other authors declare no competing interests.

Additional information

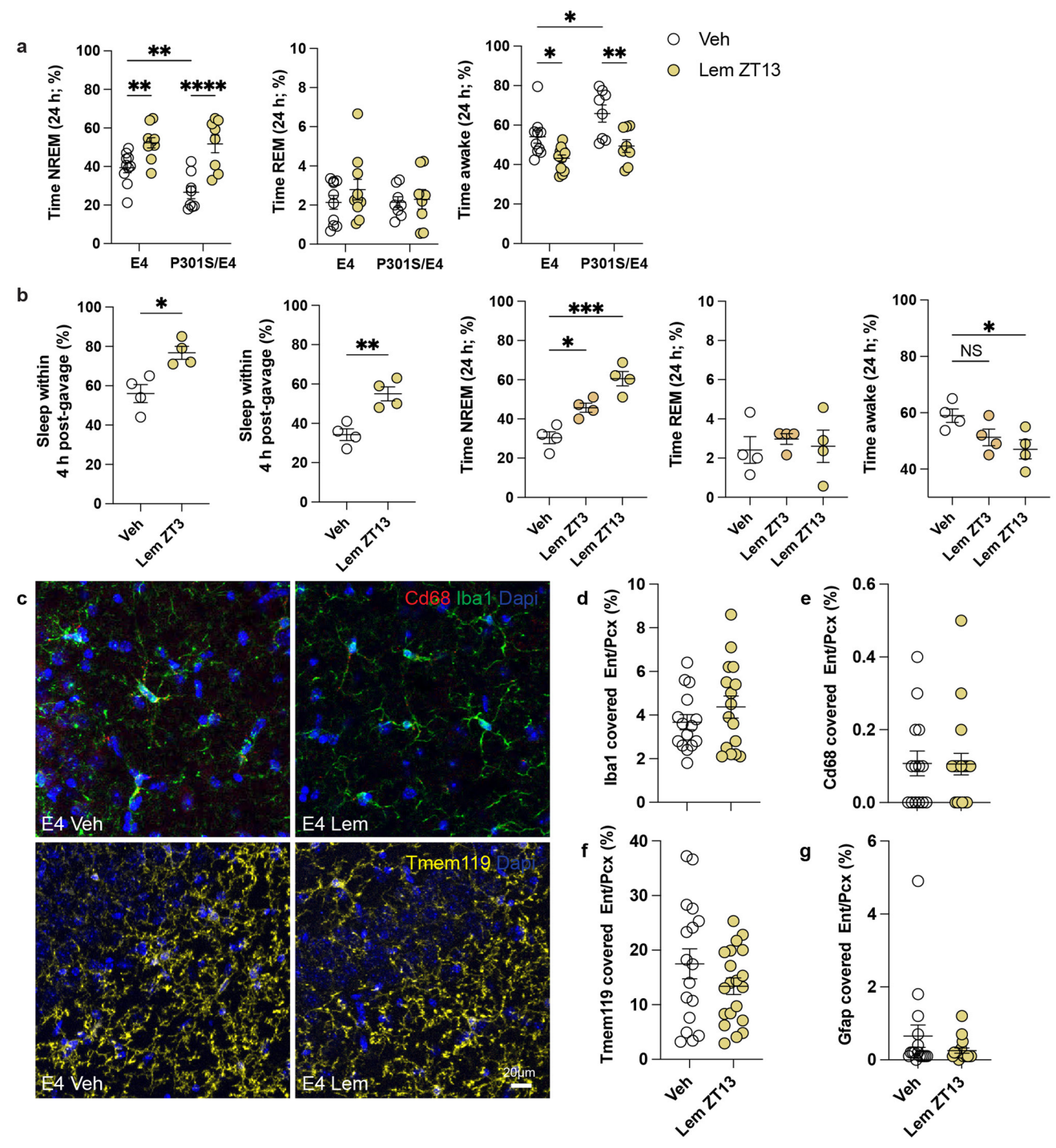
Extended data is available for this paper at https://doi.org/10.1038/s41593-025-01966-7.

Supplementary information The online version contains supplementary material available at https://doi.org/10.1038/s41593-025-01966-7.

Correspondence and requests for materials should be addressed to David M. Holtzman.

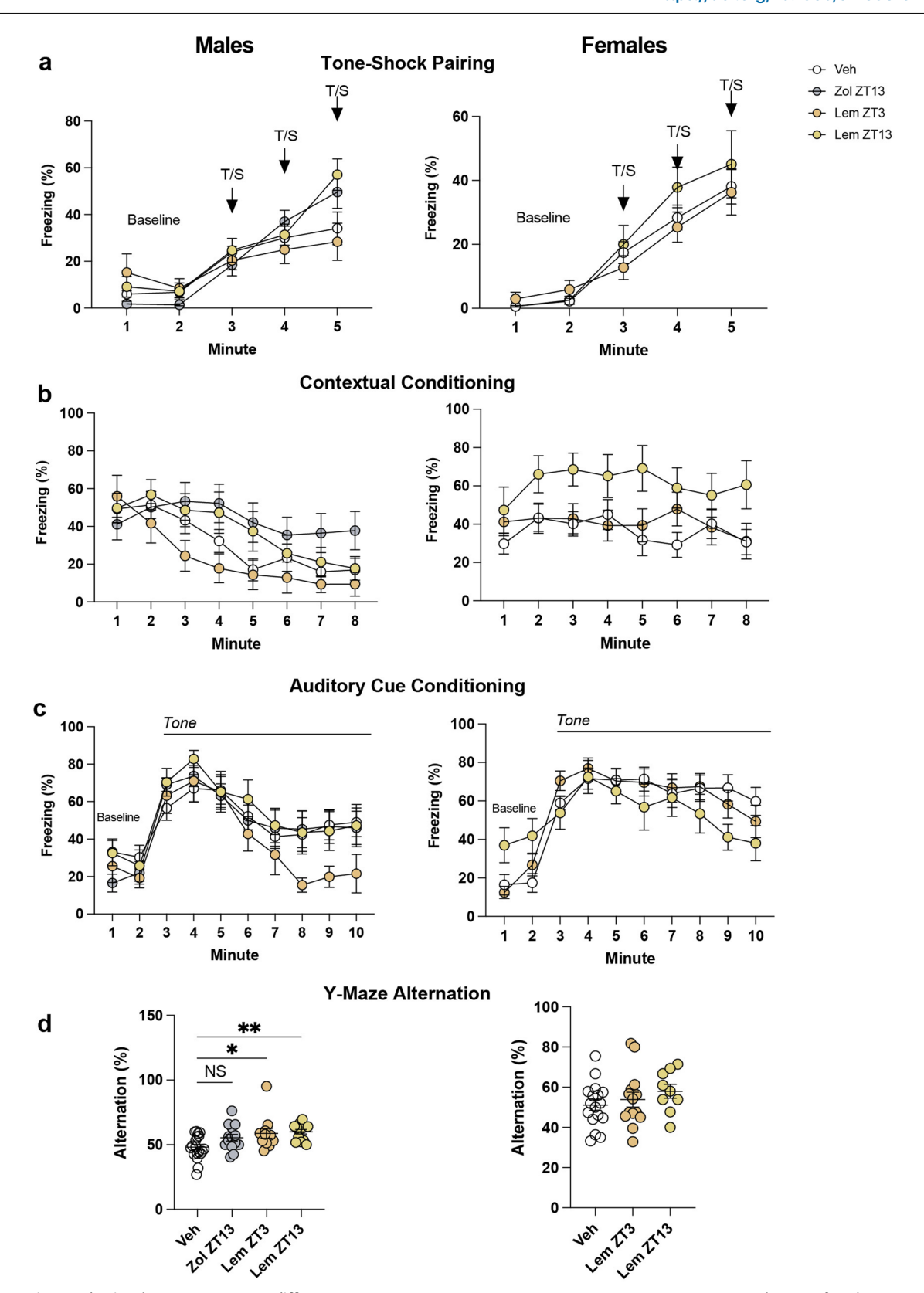
Peer review information *Nature Neuroscience* thanks Li Gan, Tara Spires-Jones and Sigrid Veasey for their contribution to the peer review of this work.

Reprints and permissions information is available at www.nature.com/reprints.



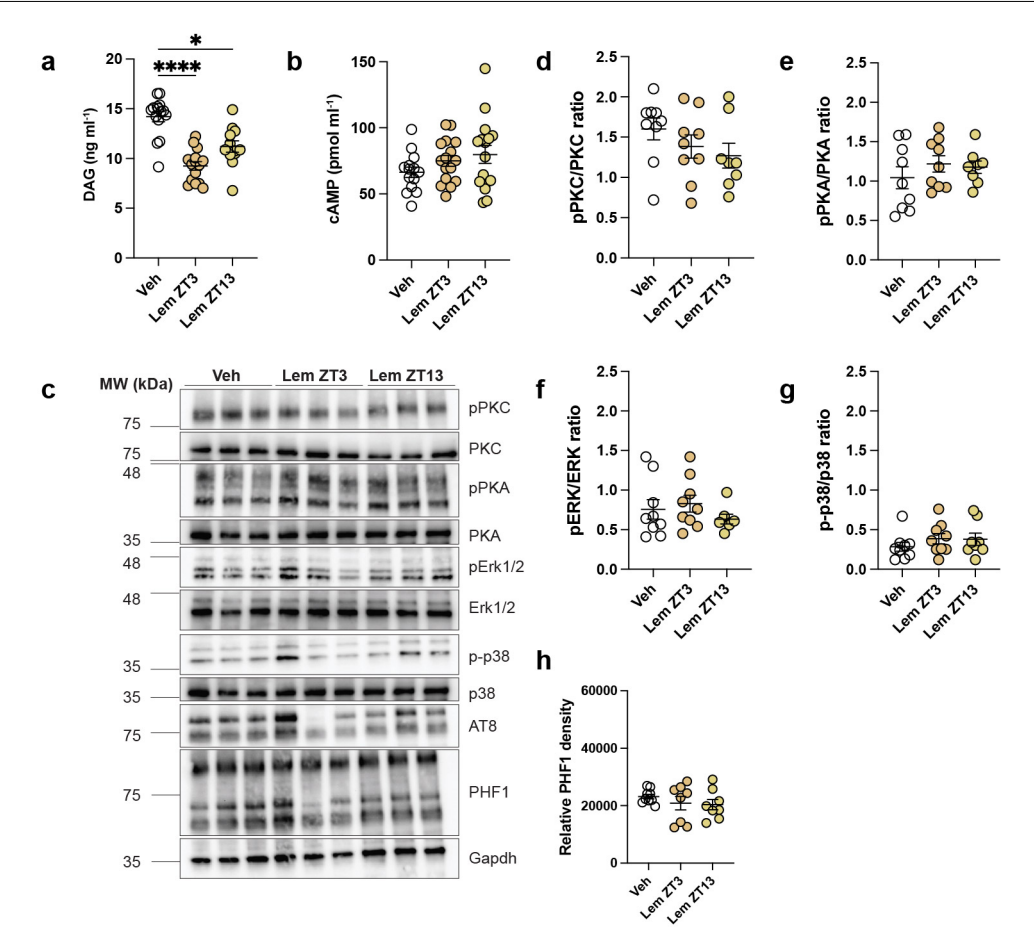
Extended Data Fig. 1 | Lemborexant influences sleep–wake behavior but does not influence reactive microglia or astroglia in non-tau transgenic E4 mice. a, EEG analyses of percentage time spent in NREM sleep (n_{E4} = 10 mice/group, $n_{P301S/E4}$ = 8 mice/group, two-way ANOVA, Fisher's LSD test), REM sleep (n_{E4} = 10 mice per group, $n_{P301S/E4}$ = 8 mice/group, two-way ANOVA, Fisher's LSD test) and awake (n_{E4} = 10 mice/group, $n_{P301S/E4}$ = 8 mice/group; two-way ANOVA and Fisher's LSD test) in Veh- and Lem-treated E4 and P301S/E4 male mice at ZT13. b, EEG analyses of percentage sleep in the first 4 h after gavage (n = 4 mice/group; two-tailed t test) as well as percentage time spent in NREM sleep (n = 4 mice/group; one-way ANOVA and Dunnett's post hoc test), REM sleep (n = 4 mice/group;

Kruskal–Wallis test) and awake (n = 4 mice/group; one-way ANOVA and Dunnett's post hoc test) in female P301S/E4 mice. **c**, Representative confocal images of Iba1 (green), Cd68 (red) and Tmem119 (yellow) stained reactive microglia in Ent/Pcx of Veh or Lem ZT13 treated E4 male mice. Scale bar, 20 μ m. **d**–**g**, Quantifications as labeled (Iba1: $n_{\rm Veh}$ = 15, $n_{\rm Lem ZT13}$ = 16, two-tailed t test; Cd68: $n_{\rm Veh}$ = 14, $n_{\rm Lem ZT13}$ = 18, two-tailed t test, p = 0.9721; Tmem119: $n_{\rm Veh}$ = 17, $n_{\rm Lem ZT13}$ = 20, two-tailed t test; Gfap: $n_{\rm Veh}$ = 16, $n_{\rm Lem ZT13}$ = 17, two-tailed t test). For detailed statistical information, see Supplementary Table 1. Data represent mean \pm s.e.m. of biological replicates; *P< 0.05, *P< 0.01, ***P< 0.001, and ****P<0.0001.



Extended Data Fig. 2| **Behavioral assessment across different treatment groups in P301S/E4 mice. a**, Percentage freezing quantified during tone–shock/pairing (males: $n_{\text{Veh}} = 19$, $n_{\text{ZoI} ZT13} = 14$, $n_{\text{Lem} ZT3} = 12$, $n_{\text{Lem} ZT13} = 13$, two-way ANOVA, Dunnett's post hoc test; females: $n_{\text{Veh}} = 17$, $n_{\text{Lem} ZT3} = 15$, $n_{\text{Lem} ZT13} = 9$, two-way ANOVA, Dunnett's post hoc test); **b**, contextual conditioning (males: $n_{\text{Veh}} = 19$, $n_{\text{ZoI} ZT13} = 14$, $n_{\text{Lem} ZT3} = 12$, $n_{\text{Lem} ZT13} = 13$, two-way ANOVA, Dunnett's post hoc test; females: $n_{\text{Veh}} = 17$, $n_{\text{Lem} ZT3} = 15$, $n_{\text{Lem} ZT13} = 9$, two-way ANOVA, Dunnett's post hoc test); **c**, auditory cue conditioning (males: $n_{\text{Veh}} = 19$, $n_{\text{ZoI} ZT13} = 14$, $n_{\text{Lem} ZT3} = 9$,

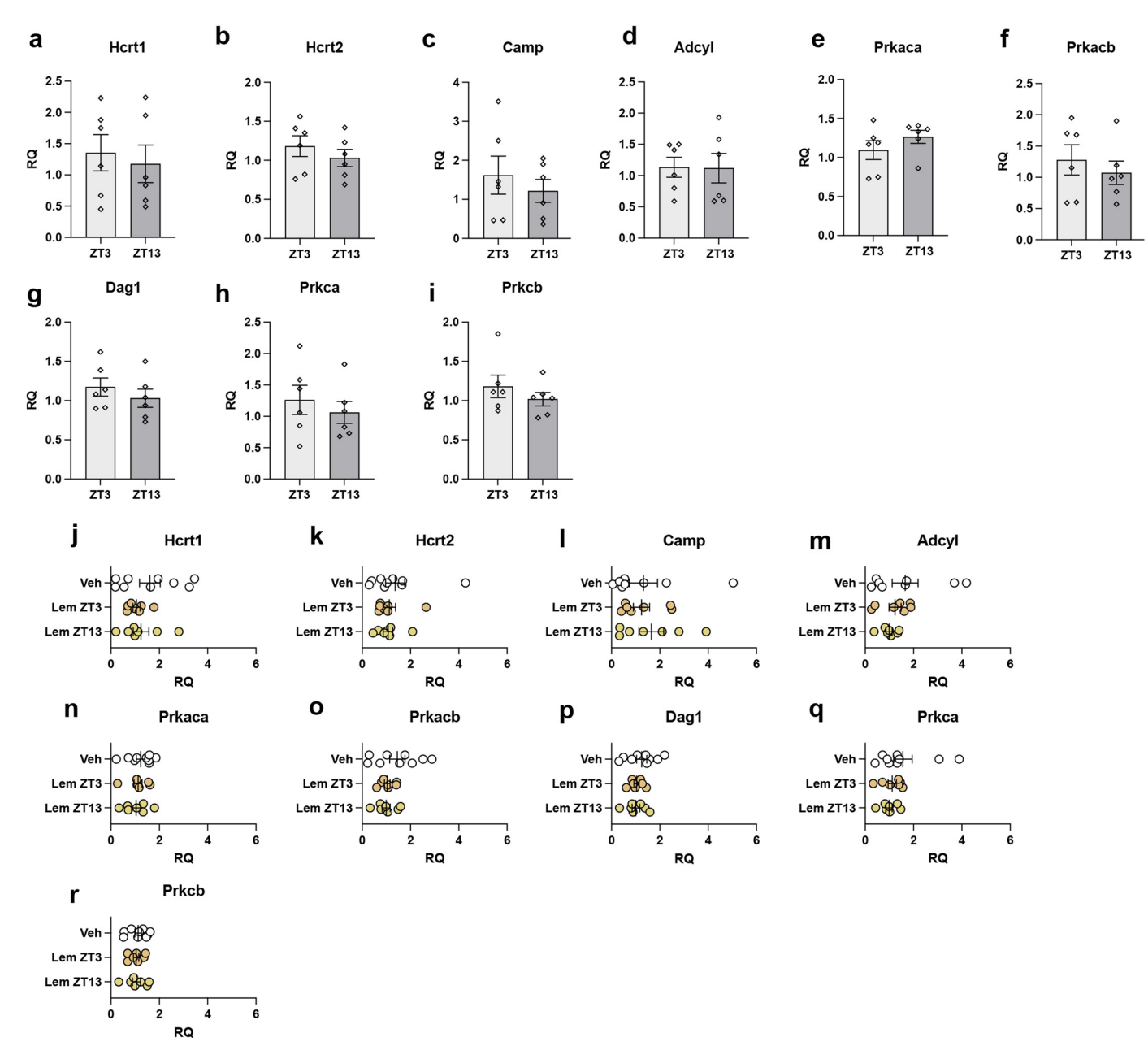
 $\begin{aligned} &n_{\text{Lem ZT13}}=13, \text{two-way ANOVA, Dunnett's post hoc test; females: } &n_{\text{Veh}}=17, \\ &n_{\text{Lem ZT3}}=15, &n_{\text{Lem ZT13}}=9, \text{two-way ANOVA, Dunnett's post hoc test). } &\textbf{d}, \text{Percentage alternation rate quantified in Y-maze alternation test (males: } &n_{\text{Veh}}=19, &n_{\text{Zol ZT13}}=14, \\ &n_{\text{Lem ZT3}}=12, &n_{\text{Lem ZT13}}=13, &\text{one-way ANOVA, Dunnett's post hoc test; females: } \\ &n_{\text{Veh}}=17, &n_{\text{Lem ZT13}}=14, &n_{\text{Lem ZT13}}=9, &\text{one-way ANOVA). For detailed statistical information, see Supplementary Table 1. Data represent mean \pm s.e.m. in biological replicates. *P < 0.05, and ** P < 0.01. \end{aligned}$



Extended Data Fig. 3 | Orexin receptor antagonism does not influence cAMP/ PKA-mediated phosphorylation of tau in P301S/E4 female mice. a, $\rm DAG$

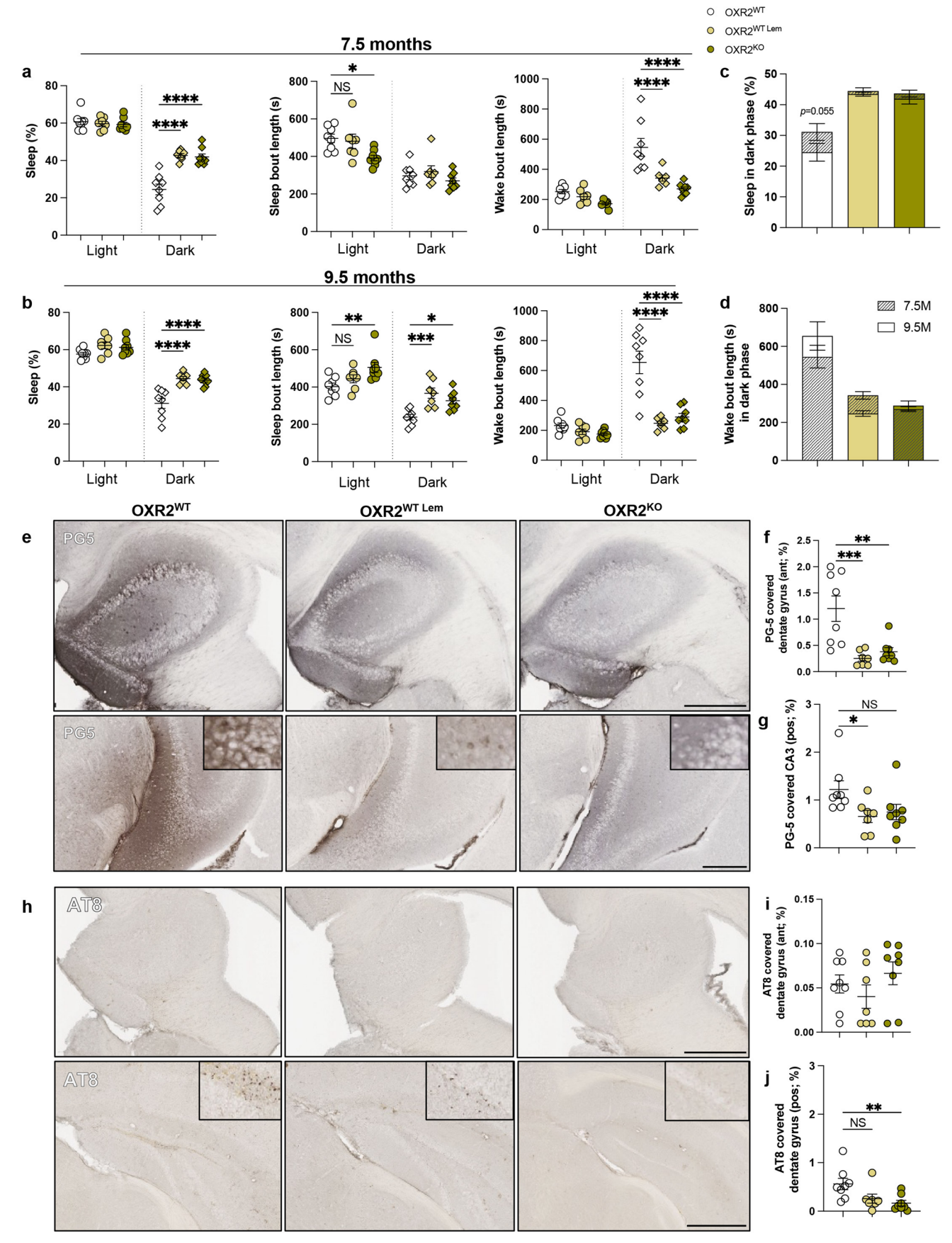
 $(n_{\text{Veh}}=15, n_{\text{Lem ZTI3}}=15, n_{\text{Lem ZTI3}}=12; Kruskal-Wallis and Dunn's post hoc test); \\ \boldsymbol{b}, cAMP (n_{\text{Veh}}=14, n_{\text{Lem ZTI3}}=16, n_{\text{Lem ZTI3}}=16; one-way ANOVA and Dunnett's post hoc test) ELISAs of RIPA-soluble Ent/Pcx extracts. <math display="inline">\boldsymbol{c}$, Immunoblots of RIPA-soluble Ent/Pcx brain extracts from Veh- and Lem-treated female P301S/E4 mice (n=3 mice/group). $\boldsymbol{d}-\boldsymbol{h}$, Quantification of the western blot intensity of protein kinases and cell signaling proteins (for \boldsymbol{d} , \boldsymbol{e} and $\boldsymbol{g}-n_{\text{Veh}}=9, n_{\text{Lem ZTI3}}=9, n_{\text{Lem ZTI3}}=8;$

for $\mathbf{f} - \mathbf{n}_{\text{Veh}} = 9$, $\mathbf{n}_{\text{Lem ZT3}} = 9$, $\mathbf{n}_{\text{Lem ZT13}} = 7$; for $\mathbf{h} - \mathbf{n}_{\text{Veh}} = 9$, $\mathbf{n}_{\text{Lem ZT3}} = 8$, $\mathbf{n}_{\text{Lem ZT3}} = 8$). All proteins were first normalized to Gapdh, and the ratio of phosphorylated to their corresponding unphosphorylated form was then calculated. PHF1 was normalized to Gapdh. ($\mathbf{d} - \text{Kruskal-Wallis test}$ and Dunn's post hoc test; $\mathbf{e} - \text{one-way ANOVA}$, Dunnett's post hoc test; $\mathbf{f} - \text{one-way ANOVA}$, Dunnett's post hoc test; $\mathbf{g} - \text{Kruskal-Wallis}$ test and Dunn's post hoc test; $\mathbf{h} - \text{one-way ANOVA}$, Dunnett's post hoc test). For detailed statistical information, see Supplementary Table 1. Data represent mean \pm s.e.m. of biological replicates. *P< 0.05, and ****P< 0.0001.



Extended Data Fig. 4 | **Gene expression levels of orexin-mediated GPCR signaling molecules. a–i,** Gene expression levels of orexin receptors and downstream effectors in naïve male P301S/E4 mice compared at ZT3 and ZT13 (n = 6 mice/group; **a–d, f–i,** two-tailed t test; **e**—Mann–Whitney test), and (**j–r**) Veh- and Lem-treated male mice (**j**– n_{Veh} = 9, $n_{Lem\ ZT3}$ = 7, $n_{Lem\ ZT3}$ = 7; one-way ANOVA and Dunnett's post hoc test; \mathbf{k} – n_{Veh} = 9, $n_{Lem\ ZT3}$ = 7, $n_{Lem\ ZT3}$ = 7; Kruskal–Wallis test and Dunn's post hoc test; \mathbf{l} – n_{Veh} = 8, $n_{Lem\ ZT3}$ = 7, $n_{Lem\ ZT3}$ = 7; one-way Wallis test and Dunn's post hoc test; \mathbf{m} – n_{Veh} = 8, $n_{Lem\ ZT3}$ = 7, $n_{Lem\ ZT3}$ = 7; one-way

ANOVA and Dunnett's post hoc test; $\mathbf{n} - n_{\text{Veh}} = 9$, $n_{\text{Lem ZT3}} = 7$, $n_{\text{Lem ZT3}} = 7$; Kruskal–Wallis test and Dunn's post hoc test; $\mathbf{o} - n_{\text{Veh}} = 9$, $n_{\text{Lem ZT3}} = 7$, $n_{\text{Lem ZT3}} = 7$; one-way ANOVA and Dunnett's post hoc test; $\mathbf{p} - n_{\text{Veh}} = 9$, $n_{\text{Lem ZT3}} = 7$, $n_{\text{Lem ZT3}} = 7$; one-way ANOVA, p = 0.5522; Dunnett's post hoc test; $\mathbf{q} - n_{\text{Veh}} = 9$, $n_{\text{Lem ZT3}} = 7$, $n_{\text{Lem ZT3}} = 7$; Kruskal–Wallis and Dunn's post hoc test; $\mathbf{r} - n_{\text{Veh}} = 9$, $n_{\text{Lem ZT3}} = 7$, $n_{\text{Lem ZT3}} = 7$; one-way ANOVA and Dunnett's post hoc test). For detailed statistical information, see Supplementary Table 1. Data represent mean \pm s.e.m. of biological replicates.



Extended Data Fig. 5 | See next page for caption.

$\label{lem:condition} Extended \ Data \ Fig. \ 5 \ | \ Pharmacological \ or \ genetic \ lack \ of \ or \ exin \ receptor \ signaling \ alters \ sleep-wake \ behavior \ and \ decreases \ tau \ propagation.$

a, Sleep-wake behavior quantified by percentage sleep (two-way ANOVA and Sidak's post hoc test), sleep bout lengths (two-way ANOVA and Sidak's post hoc test) and wake bout lengths (two-way ANOVA and Sidak's post hoc test) during the light and dark phase at 7.5 M ($n_{OXR2-WT} = 8$, $n_{OXR2-WT} = 7$, $n_{OXR2-KO} = 8$) male mice. **b**, Sleep-wake behavior quantified by percentage sleep (two-way ANOVA and Sidak's post hoc test), sleep bout lengths (two-way ANOVA and Sidak's post hoc test) and wake bout lengths (two-way ANOVA and Sidak's post hoc test) during the light and dark phase at 9.5 M ($n_{OXR2-WT} = 8$, $n_{OXR2-WT} = 7$, $n_{OXR2-KO} = 8$) in male mice. **c**, Percentage sleep in dark phase compared between mice at 7.5 M and 9.5 M (both timepoints: $n_{OXR2-WT} = 8$, $n_{OXR2-WT} = 7$, $n_{OXR2-KO} = 8$; two-way ANOVA and Bonferroni's post hoc test). **d**, Wake bout lengths compared between mice

at 7.5 M and 9.5 M during dark phase (both timepoints: $n_{\text{OXR2-WT}} = 8$, $n_{\text{OXR2-WTLem}} = 7$, $n_{\text{OXR2-WT}} = 8$, two-way ANOVA and Bonferroni's post hoc test). **e**, Representative images of PG5-stained anterior (ant; top) and posterior (pos; bottom) Hpc. Scale bar, 500 µm. **f**, Percentage PG5-covered dentate gyrus quantified anterior ($n_{\text{OXR2-WT}} = 8$, $n_{\text{OXR2-WTLem}} = 7$, $n_{\text{OXR2-KO}} = 8$ male mice; one-way ANOVA and Dunnett's post hoc test); **g**, posterior to the seeding site (one-way ANOVA and Dunnett's post hoc test). **h**, Representative images of AT8-stained anterior and posterior Hpc. Scale bar, 500 µm. **i**, Percentage AT8-covered dentate gyrus quantified anterior ($n_{\text{OXR2-WT}} = 8$, $n_{\text{OXR2-WTLem}} = 7$, $n_{\text{OXR2-KO}} = 8$ male mice; one-way ANOVA and Dunnett's post hoc test); **j**, posterior to the seeding site (Kruskal-Wallis test and Dunn's post hoc test). For detailed statistical information, see Supplementary Table 1. Data represent mean \pm s.e.m. in biological replicates. *P< 0.05, **P< 0.01, ***P<0.001. and ****P<0.001.

nature portfolio

Corresponding author(s):	David M. Holtzman
Last updated by author(s):	Feb 22, 2025

Reporting Summary

Nature Portfolio wishes to improve the reproducibility of the work that we publish. This form provides structure for consistency and transparency in reporting. For further information on Nature Portfolio policies, see our <u>Editorial Policies</u> and the <u>Editorial Policy Checklist</u>.

For all statistical analyses, confirm that the following items are present in the figure legend, table legend, main text, or Methods section.

\sim				
✓.	ナつ	١+.	ıct	$\Gamma \subset C$
J	LΟ	ΙL	ıσι	ics

n/a	Confirmed
	$oxed{oxed}$ The exact sample size (n) for each experimental group/condition, given as a discrete number and unit of measurement
	🔀 A statement on whether measurements were taken from distinct samples or whether the same sample was measured repeatedly
	The statistical test(s) used AND whether they are one- or two-sided Only common tests should be described solely by name; describe more complex techniques in the Methods section.
	A description of all covariates tested
	🔀 A description of any assumptions or corrections, such as tests of normality and adjustment for multiple comparisons
	A full description of the statistical parameters including central tendency (e.g. means) or other basic estimates (e.g. regression coefficient) AND variation (e.g. standard deviation) or associated estimates of uncertainty (e.g. confidence intervals)
	For null hypothesis testing, the test statistic (e.g. <i>F</i> , <i>t</i> , <i>r</i>) with confidence intervals, effect sizes, degrees of freedom and <i>P</i> value noted <i>Give P values as exact values whenever suitable.</i>
\boxtimes	For Bayesian analysis, information on the choice of priors and Markov chain Monte Carlo settings
\boxtimes	For hierarchical and complex designs, identification of the appropriate level for tests and full reporting of outcomes
\boxtimes	Estimates of effect sizes (e.g. Cohen's <i>d</i> , Pearson's <i>r</i>), indicating how they were calculated

Our web collection on statistics for biologists contains articles on many of the points above.

Software and code

Policy information about availability of computer code

Data collection

Non-invasive assesment of sleep/wake behavior was achieved using PiezoSleep SleepStats software (Signal Solutions, v2.18). Bilateral cortical EEG signals were acquired by a P511K A.C. Preamplifier (Grass-Telefactor Instruments, Warwick, RI USA), digitized with a BIOPAC MP150, recorded digitally using the BIOPAC's AcqKnowlege 5.0 software. Plasma NfL concentration was measured with NF-Light Simoa Assay Advantage kit on a Samoa HD analyzer (Quanterix). Immunohistochemistry and cresyl violet images were obtained by a NanoZoomer microscope (Hamamatsu Photonics). Immunofluorescence images were acquired using a Leica Stellaris 5 confocal microscope and the Leica Application Suite X software (4.2.1.23810). Western blot membranes were imaged by ChemiDoc Imaging Systems (Bio-Rad).

Data analysis

EEG was processed and analyzed in MATLAB (MathWorks). Volumetric analysis was performed using NDP.view 2. Immunofluorescence stainings were analyzed using FIJI (ImageJ2, 2.14.0/1.54f). Behavioral freezing was analyzed using FreezeFrame image analysis software (Actimetrics, Evanston, IL). For RNAseq, RNA quality was controlled using Bioanalyzer prior to Next Generation Sequencing by Clontech SMARTer. RNA-seq reads were then aligned and quantitated to the Ensembl release 101 primary assembly with an Illumina DRAGEN Bio-IT onpremise server running software (3.9.3-8). All gene counts were then imported into R package (4.1.1). EdgeR (3.36.0) and TMM normalization size factors were calculated to adjust for samples for differences in library size. The TMM size factors and the matrix of counts were then imported into the R/Bioconductor package Limma (3.50.0). Weighted likelihoods based on the observed mean-variance relationship of every gene and sample were then calculated for all samples with the voomWithQualityWeights function and were fitted using a Limma generalized linear model with additional unknown latent effects as determined by surrogate variable analysis (sva package version 3.42.0). GraphPad Prism 10.0 was utilized for all statistical analyses.

For manuscripts utilizing custom algorithms or software that are central to the research but not yet described in published literature, software must be made available to editors and reviewers. We strongly encourage code deposition in a community repository (e.g. GitHub). See the Nature Portfolio guidelines for submitting code & software for further information.

Data

Policy information about availability of data

All manuscripts must include a data availability statement. This statement should provide the following information, where applicable:

- Accession codes, unique identifiers, or web links for publicly available datasets
- A description of any restrictions on data availability
- For clinical datasets or third party data, please ensure that the statement adheres to our policy

Numerical source data files are available as supplementary data files. RNA Sequencing data are publicly available from the Gene Expression Omnibus (GEO) under accession code GSE283736.

Research involving human participants, their data, or biological material

Policy information about studies with <u>human participants or human data</u>. See also policy information about <u>sex, gender (identity/presentation)</u>, and sexual orientation and race, ethnicity and racism.

Reporting on sex and gender	No human participants were involved in the study
Reporting on race, ethnicity, or other socially relevant groupings	No human participants were involved in the study
Population characteristics	No human participants were involved in the study
Recruitment	No human participants were involved in the study
Ethics oversight	No human participants were involved in the study

Note that full information on the approval of the study protocol must also be provided in the manuscript.

Field-specific reporting

	1 10		1.41		1 (1. 1	
Please select the one below that is the best fit for	vour research It v	VOLLARE NOT SUIPE	read the annror	ariate sections	hetore making volir selec	ction
ricase select the one below that is the best ht for	your rescurent in	you are not sare,	redu tile approp	Jilate Sections	before making your seree	ction.

☐ Behavioural & social sciences ☐ Ecological, evolutionary & environmental sciences

For a reference copy of the document with all sections, see <u>nature.com/documents/nr-reporting-summary-flat.pdf</u>

Life sciences study design

All studies must disclose on these points even when the disclosure is negative.

Sample size

No statistical methods were used to pre-determine sample sizes. However, our sample sizes were based on experience from our previous findings. For example, sample size for sleep analysis were based on on our prior experience with sleep analysis in the P301S mouse model (Holth et al., 2017 Ann Clin Transl Neurol). Similarly, sample sizes for tau and neurodegeneration pathology was based on our prior experience with characterization of the P301S/E4 model (Shi et al., 2017 Nature).

Data exclusions

Samples were excluded from the sleep experiments if the data demonstrated significant noise after filtration, compromising its reliability. Additionally, mice that were too sick to undergo behavioral assessments were excluded to prioritize animal welfare and preserve the accuracy and consistency of the experimental results. For immunohistochemistry experiments, samples were excluded if the tissue integrity was compromised in one or more of the replicates. For biochemistry experiments, samples were excluded if the sample quality was compromised by, for example, impurity, low protein yield, or pipetting inconsistencies across technical replicates.

Replication

Biological replicates were performed for all experiments and reported in the figure legends. All sleep analyses were analyzed by at least 2 different experimenters. All ELISA measurements were performed in technical duplicates. For all immunohistochemistry experiments, each staining was performed on 3 sections per mouse. All experiments except for thee immunoblots were independently replicated at least twice by more than one investigator, with results obtained months apart to confirm reproducibility, with each experiment yielding similar results. All immunoblots represent biological replicates and were performed once due to limited tissue availability after other listed biochemical experiments.

Randomization

For all animal experiments, mice were randomly assigned to experimental groups that were matched by sex, littermate, and age using the RAND function in Microsoft Excel following genotyping.

Blinding

All identifying numbers for the mice were pseudonymized, and the investigator remained blinded to these identifiers, ensuring that all experiments and analyses were conducted in a blinded manner. Investigators were unblinded for statistical analyses.

Reporting for specific materials, systems and methods

		materials, experimental systems and methods used in many studies. Here, indicate whether each material e not sure if a list item applies to your research, read the appropriate section before selecting a response.	
Materials & experime	ental systems	Methods	
n/a Involved in the study		n/a Involved in the study	
☐ ☐ Antibodies		ChIP-seq	
Eukaryotic cell line	S	Flow cytometry	
Palaeontology and		MRI-based neuroimaging	
	0,	With-based flediolifiaging	
Animals and other	organisms		
Clinical data			
Dual use research	of concern		
Plants			
I			
Antibodies			
Antibodies used Primary antibodies were us IBA1 (1:500; Cat#019-1974			
	, ,	228, Lot#s7C7G2P59, Novus Biologicals)	
	CD68 (1:1000; Cat#FA-11, L	ot#1807, BioRad) 10, Lot#1, Cell Signaling Technology)	
, · · · ·		dect, Lot#6114-43-01, InvivoGen)	
GFAP (1:2000; Cat#2E1.E9 Alexa Flour 488-conjugated, Lot#2211022, BioLegend)			
APOE (1:300; Cat#D7I9N, Lot#4, Cell Signaling)			
	, .	0, Lot#WK329091, Thermo Fisher Scientific) 15, Lot#3836436, Merck Millipore)	
	, ,	t#MN1020B, Lot#VA2912562Z, Thermo Fisher Scientific)	
	MC1 (1:500, kindly gifted by		
PG5 (1:500, kindly gifted by Dr. Peter PHF1 (1:1000, kindly gifted by Dr. Pe			
		by Dr. Peter Davies)	
	PKC (1:1000, Cat#46809S, L	_ot#1, Cell Signaling Technology)	
	phospho-PKC (1:1000, Cat#	ł38938S, Lot#1, Cell Signaling Technology)	
	, ,	ot#3, Cell Signaling Technology)	
		S, Lot#35, Cell Signaling Technology)	
	phospho-Erk (1:1000, Cat#/	4370S. Lot#30. Cell Signaling Technology)	

Secondary antibodies were used as follows:

p38 (1:1000, Cat#8690S, Lot#27, Cell Signaling Technology) phospho-p38 (1:1000, Cat#4511S, Lot#13, Cell Signaling Technology) GAPDH (1:2000, Cat#HRP-60004, Lot#21010938, Proteintech)

Donkey-anti-rabbit IgG (H+L)-AlexaFluor647 (1:1000, Cat#A31573, Lot#2420695, Thermo Fisher Scientific) Donkey-anti-rabbit IgG (H+L)-AlexaFluor594 (1:1000, Cat#A21207, Lot#2441375, Thermo Fisher Scientific) Donkey-anti-goat IgG (H+L)-AlexaFluor594 (1:1000, Cat#A11058, Lot#2445414, Thermo Fisher Scientific) Donkey-anti-goat IgG (H+L)-AlexaFluor647 (1:1000, Cat#A21447, Lot#2465096, Thermo Fisher Scientific) Donkey-anti-rat IgG(H+L)- AlexaFluor488 (1:1000, Cat#A21208, Lot#2482958, Thermo Fisher Scientific) Goat-anti-guinea pig IgG(H+L)-AlexaFluor488 (1:500, Cat#A11073, Lot#2087691, Thermo Fisher Scientific) Goat-anti-rabbit IgG (H+L)-AlexaFluor594 (1:500, Cat#A11037, Lot#2160431, Thermo Fisher Scientific)

Goat-anti rabbit HRP (1:5000, Cat#31460, Lot#YH381824, Thermo Fisher Scientific) Goat anti-mouse HRP (1:200, Cat#31430, Lot#4F375332, Thermo Fisher Scientific)

Validation

Wild-type mice were used as negative controls for the PG5, MC1 and AT8 tau staining experiments. PG5 and MC1 antibodies have been widely used in the field and were first published by Dr Peter Davies' lab (Jicha et al., 1997, J Neurosci Res; and Jicha et al., 1999 J Neurosci). All other antibodies are commercially available and have been tested in mice.

1. IBA1 (Cat#019-19741, Lot#LEF4660, Fujifilm Wako)

Validation Methods:

Verified for immunocytochemistry (IHC)

Used as a standard microglia marker

Manufacturer recommends a dilution of 1:500-1:1,000

Tested for specific staining of microglial processes

Manufacturer's Validation Statement:

"Anti-Iba1 antibody is useful for immunohistochemical staining of microglia. It is known to react specifically with microglia in the central nervous system."

Manufacturer's Website:

https://labchem-wako.fujifilm.com/us/product/detail/W01W0101-1974.html

2. IBA1 (Cat#NB100-1028, Lot#s7C7G2P59, Novus Biologicals)

Validation Methods:

Tested for Western Blot (WB), Immunohistochemistry (IHC), and Immunofluorescence (IF)

Detects a 16 kDa band in human frontal cortex, mouse brain, rat brain, and mouse lymph node lysates

Dual ISH-IHC validation in literature (PMID: 31220182)

Manufacturer's Validation Statement:

"This Iba1 antibody has been validated for multiple applications, including Western Blot and Immunohistochemistry, demonstrating specific detection of microglial activation in various tissue samples."

Manufacturer's Website:

https://www.novusbio.com/products/aif-1-iba1-antibody_nb100-1028

Register ID:

AB 521594

Antibodypedia Link:

https://www.antibodypedia.com/gene/27285/AIF1/antibody/73259/NB100-1028

3. CD68 (Cat#FA-11, Lot#1807, BioRad)

Validation Methods:

Validated for use in IHC on paraffin-embedded tissues

Specific staining of macrophages in various tissues

Flow cytometry validation available

Manufacturer's Validation Statement: "FA-11 monoclonal antibody specifically detects murine CD68, a widely used macrophage marker, validated for IHC applications."

Manufacturer's Website: https://www.bio-rad-antibodies.com/cd68-antibody-fa-11-mouse-monoclonal-mca1957.html

Register ID:AB_324503

Antibodypedia Link: https://www.antibodypedia.com/gene/27242/CD68/antibody/67324/MCA1957

4. TMEM119 (Cat#E3E1O, Lot#1, Cell Signaling Technology)

Validation Methods:

Tested for IHC and Western Blot (WB)

Specific staining of microglia with no cross-reactivity in neurons or astrocytes

WB validation shows a single band at the expected molecular weight

Manufacturer's Validation Statement:

"This TMEM119 antibody detects endogenous levels of total TMEM119 protein and is validated for applications including immunohistochemistry and Western blot."

Manufacturer's Website:

https://www.cellsignal.com/products/primary-antibodies/tmem119-antibody/84880

Register ID:

AB 2799362

Antibodypedia Link:

https://www.antibodypedia.com/gene/41933/TMEM119/antibody/806249/84880

5. Clec7a (Cat#mabg-mdect, Lot#6114-43-01, InvivoGen)

Validation Methods:

Verified for use in flow cytometry (FC) and WB

Recognizes mouse Dectin-1, a C-type lectin receptor

Specific binding confirmed in bone marrow-derived macrophages

Manufacturer's Validation Statement:

"This monoclonal antibody binds specifically to mouse Dectin-1 and is validated for applications such as flow cytometry and immunoblotting."

Manufacturer's Website:

https://www.invivogen.com/mabg-mdect

Register ID:

Not available

Antibodypedia Link:

https://www.antibodypedia.com/gene/26343/CLEC7A/antibody/846663/mabg-mdect

6. GFAP (Cat#2E1.E9 Alexa Fluor 488-conjugated, Lot#2211022, BioLegend)

Validation Methods:

Validated for flow cytometry, IHC, and IF

Recognizes glial fibrillary acidic protein (GFAP), an astrocyte marker

Specificity confirmed by knockdown and knockout studies

Manufacturer's Validation Statement:

"This GFAP antibody is conjugated to Alexa Fluor 488 for high-sensitivity detection in immunofluorescence and flow cytometry applications."

Manufacturer's Website:

https://www.biolegend.com/en-us/products/gfap-antibody-2e1e9-alexa-fluor-488-13481

Register ID:

AB_2564502

Antibodypedia Link:

https://www.antibodypedia.com/gene/27377/GFAP/antibody/716798/829401

7. APOE (Cat#D7I9N, Lot#4, Cell Signaling Technology)

Validation Methods:

Tested for IHC, WB, and Immunocytochemistry (ICC)

WB validation confirms a single band at the expected molecular weight

Immunofluorescence (IF) confirms specific localization in human and mouse tissue

Manufacturer's Validation Statement:

"This antibody detects endogenous levels of APOE and is validated for applications including Western blot, immunohistochemistry, and immunocytochemistry."

Manufacturer's Website:

https://www.cellsignal.com/products/primary-antibodies/apoe-antibody/13366

Register ID:

AB_2687463

Antibodypedia Link:

https://www.antibodypedia.com/gene/282/APOE/antibody/762312/13366

8. PSD-95 (Cat#51-6900, Lot#WK329091, Thermo Fisher Scientific)

Validation Methods:

Tested in WB and ICC

Western blot confirms specificity at ~95 kDa

Validated for detecting postsynaptic density protein in neurons

Manufacturer's Validation Statement:

"This PSD-95 antibody has been validated for use in immunocytochemistry and Western blot, specifically detecting postsynaptic density protein-95 in neuronal tissue."

Manufacturer's Website:

https://www.thermofisher.com/antibody/product/PSD-95-Antibody-7E3-1B8-Monoclonal/51-6900

Register ID:

AB_2533903

Antibodypedia Link:

https://www.antibodypedia.com/gene/25677/DLG4/antibody/167423/51-6900

9. VGLUT1 (Cat#AB5905, Lot#3836436, Merck Millipore)

Validation Methods:

Validated for IHC and WB

Western blot confirms specificity at ~55 kDa

Recognized as a specific marker for glutamatergic synapses

Manufacturer's Validation Statement:

"This antibody is validated for detecting VGLUT1 in brain tissue sections and Western blot applications, providing reliable identification of glutamatergic synapses."

Manufacturer's Website:

https://www.sigmaaldrich.com/US/en/product/mm/ab5905

Register ID:

AB_2301751

Antibodypedia Link:

https://www.antibodypedia.com/gene/24822/SLC17A7/antibody/71584/AB5905

10. AT8-Biotinylated (Cat#MN1020B, Lot#VA2912562Z, Thermo Fisher Scientific)

Validation Methods:

Validated for IHC and WB

Recognizes phosphorylated tau at Ser202/Thr205

Confirmed specificity via knockout studies

Manufacturer's Validation Statement:

"The AT8 antibody is specific for phosphorylated tau and has been validated for immunohistochemistry and Western blot applications."

Manufacturer's Website:

https://www.thermofisher.com/antibody/product/Phospho-Tau-Ser202-Thr205-Antibody-AT8-Monoclonal/MN1020B

Register ID:

AB_223647

Antibodypedia Link:

https://www.antibodypedia.com/gene/41281/MAPT/antibody/864144/MN1020B

11. PKC (Cat#46809S, Lot#1, Cell Signaling Technology)

Validation Methods:

Validated for WB and IHC

Recognizes multiple isoforms of protein kinase C (PKC)

Western blot confirms expected molecular weight bands

Manufacturer's Validation Statement:

"This antibody detects endogenous levels of total PKC and is validated for applications including Western blot and immunohistochemistry."

Manufacturer's Website:

https://www.cellsignal.com/products/primary-antibodies/pkc-antibody/46809

Register ID:

AB 2799359

Antibodypedia Link:

https://www.antibodypedia.com/gene/27087/PRKCA/antibody/869222/46809

12. Phospho-PKC (Cat#38938S, Lot#1, Cell Signaling Technology)

Validation Methods:

Validated for WB and IHC

Recognizes phosphorylated PKC at specific activation sites

Western blot detects phosphorylation-dependent mobility shifts

Manufacturer's Validation Statement:

"This antibody detects PKC phosphorylated at activation loop sites and has been validated for Western blot and immunohistochemistry applications."

Manufacturer's Website:

https://www.cellsignal.com/products/primary-antibodies/phospho-pkc-alpha-beta-delta-theta-ser643-ser676-antibody/38938 Register ID:

AB_2799360

Antibodypedia Link:

https://www.antibodypedia.com/gene/27087/PRKCA/antibody/869223/38938

13. PKA (Cat#4782S, Lot#3, Cell Signaling Technology)

Validation Methods:

WB and IHC validation

Recognizes catalytic subunits of PKA

Specificity confirmed via knockout and inhibition studies

Manufacturer's Validation Statement:

"This antibody detects endogenous levels of total PKA catalytic subunits and is validated for WB and IHC applications."

Manufacturer's Website:

https://www.cellsignal.com/products/primary-antibodies/pka-catalytic-subunit-antibody/4782

Register ID:

AB_2090260

Antibodypedia Link:

https://www.antibodypedia.com/gene/27084/PRKACA/antibody/869224/4782

14. ERK1/2 (Cat#4695S, Lot#35, Cell Signaling Technology)

Validation Methods:

WB, IHC, and IF validation

Detects ERK1 and ERK2 isoforms

Knockout and siRNA controls confirm specificity

Manufacturer's Validation Statement:

"This antibody detects ERK1 and ERK2 in multiple species and is validated for WB, IHC, and IF applications."

Manufacturer's Website:

https://www.cellsignal.com/products/primary-antibodies/erk1-2-antibody/4695

Register ID:

AB_390779

Antibodypedia Link:

https://www.antibodypedia.com/gene/24954/MAPK1/antibody/869225/4695

15. Phospho-ERK (Cat#4370S, Lot#30, Cell Signaling Technology)

Validation Methods:

WB, IHC, and IF validation

Detects phosphorylated ERK1/2

Knockout and inhibition studies confirm specificity

Manufacturer's Validation Statement:

"This antibody detects ERK1/2 when phosphorylated at Thr202/Tyr204 and is validated for WB, IHC, and IF."

https://www.cellsignal.com/products/primary-antibodies/phospho-p44-42-mapk-erk1-2-thr202-tyr204-antibody/4370-p44-4-thr202-tyr204-antibody/4370-p44-4-thr202-tyr204-antibody/4370-p44-4-thr202-tyr204-antibody/4370-p44-4-thr202-tyr204-antibody/4370-tyr204-antibod

Register ID:

AB_331646

Antibodypedia Link:

https://www.antibodypedia.com/gene/24954/MAPK1/antibody/869226/4370

16. p38 (Cat#8690S, Lot#27, Cell Signaling Technology)

Validation Methods:

Validated for WB, IHC, and IF

Recognizes p38 MAPK isoforms

Specificity confirmed with knockdown and inhibition experiments

Manufacturer's Validation Statement:

"This antibody detects total p38 MAPK and is validated for use in Western blot, immunohistochemistry, and immunofluorescence."

Manufacturer's Website:

https://www.cellsignal.com/products/primary-antibodies/p38-mapk-antibody/8690

Register ID:

AB 390778

Antibodypedia Link:

https://www.antibodypedia.com/gene/5607/ MAPK14/antibody/869227/8690

17. Phospho-p38 (Cat#4511S, Lot#13, Cell Signaling Technology)

Validation Methods:

WB and IHC validation

Detects phosphorylated p38 MAPK at Thr180/Tyr182

Confirmed specificity via inhibitor treatment and siRNA

Manufacturer's Validation Statement:

"This antibody detects phosphorylated p38 MAPK and is validated for use in Western blot, immunohistochemistry, and immunofluorescence."

Manufacturer's Website:

https://www.cellsignal.com/products/primary-antibodies/phospho-p38-mapk-thr180-tyr182-antibody/4511

Register ID:

AB_389196

Antibodypedia Link:

https://www.antibodypedia.com/gene/5607/MAPK14/antibody/869228/4511

18. GAPDH (Cat#HRP-60004, Lot#21010938, Proteintech)

Validation Methods:

Validated for WB and IHC

Recognizes GAPDH in human and mouse samples

Specificity confirmed by knockout and knockdown studies

Manufacturer's Validation Statement:

"This GAPDH antibody is validated for Western blot, immunohistochemistry, and enzyme-linked immunosorbent assay (ELISA) applications."

Manufacturer's Website:

https://www.ptglab.com/products/GAPDH-Antibody-HRP-60004/

Register ID:

AB 2907094

Antibodypedia Link:

https://www.antibodypedia.com/gene/2597/GAPDH/antibody/946911/HRP-60004

Animals and other research organisms

Policy information about <u>studies involving animals</u>; <u>ARRIVE guidelines</u> recommended for reporting animal research, and <u>Sex and Gender in</u> Research

Laboratory animals

All mice were bred, maintained, and used in experiments in our specific pathogen-free (SPF) animal facility in accordance with the guidelines of the Division of Comparative Medicine under the protocol (24-0098) approved by the Institutional Animal Care Care and Use Committee (IACUC) at Washington University School of Medicine.

PS19 tau transgenic mice harboring 1N4R tau (Jax, #008169) and overexpressing human P301S tau mutation were used27. These mice have been backcrossed to C57BL/6 for more than ten generations. Human APOE4 knock-in mice were generated by replacing the mouse genomic sequence from the translation initiation codon in exon2 to the termination codon in exon4 with its human counterparts flanked by loxP sites (Huyn et al., 2019 Molecular Neurodegeneration). P301S tau transgenic mice on C57BL/6 background were crossed to human ApoE KI mice to generate P301S/E4 mice and bred for several generations to produce experimental mice.

Orexin receptor 2 knockout mice on a C57BL/6 background (Willie et al., 2003, Neuron) were rederived from cryopreserved embryos. Orexin receptor 2 wild-type and homozygous knockout male mice were used for experiments.

Wild animals

This study did not include wild animals.

Reporting on sex

Both male and female mice were used in this study and evaluated separately as male P301S/E4 mice display more robust brain atrophy than females at 9.5 months of age, based on our experience working with this model (Huyn et al., 2019 Molecular Neurodegeneration; Shi et al., 2017 Nature; Wang et al., 2021 Neuron).

Field-collected samples

This study did not include field-collected samples.

Ethics oversight

All animal procedures and protocols were in accordance with the guidelines of the Division of Comparative Medicine under the protocols (24-0098) approved by the Institutional Animal Care Care and Use Committee (IACUC) at Washington University School of Medicine.

Note that full information on the approval of the study protocol must also be provided in the manuscript.

Plants

Seed stocks

Report on the source of all seed stocks or other plant material used. If applicable, state the seed stock centre and catalogue number. If plant specimens were collected from the field, describe the collection location, date and sampling procedures.

Novel plant genotypes

Describe the methods by which all novel plant genotypes were produced. This includes those generated by transgenic approaches, gene editing, chemical/radiation-based mutagenesis and hybridization. For transgenic lines, describe the transformation method, the number of independent lines analyzed and the generation upon which experiments were performed. For gene-edited lines, describe the editor used, the endogenous sequence targeted for editing, the targeting guide RNA sequence (if applicable) and how the editor

Authentication

was applied.

Describe any authentication procedures for each seed stock used or novel genotype generated. Describe any experiments used to assess the effect of a mutation and, where applicable, how potential secondary effects (e.g. second site T-DNA insertions, mosiacism, off-target gene editing) were examined.